Geomechanics and Engineering, *Vol. 36, No. 2 (2024) 183-204*
https://doi.org/10.12989/gae.2024.36.2.183

On the elastic stability and free vibration responses of functionally graded porous beams resting on Winkler-Pasternak foundations via finite element computation

Zakaria Belabed[1,2], Abdelouahed Tounsi*[3], Mohammed A. Al-Osta[4,5], Abdeldjebbar Tounsi[2] and Hoang-Le Minh[3]

[1]*Artificial Intelligence Laboratory for Mechanical and Civil Structures, and Soil, Institute of Technology, University Center of Naama, BP 66, 45000 Naama, Algeria*
[2]*Material and Hydrology Laboratory, University of Sidi Bel Abbes, Faculty of Technology, Civil Engineering Department, Algeria*
[3]*Center for Engineering Application & Technology Solutions, Ho Chi Minh City Open University, Ho Chi Minh City, Vietnam*
[4]*Department of Civil and Environmental Engineering, King Fahd University of Petroleum & Minerals, 31261 Dhahran, Eastern Province, Saudi Arabia*
[5]*Interdisciplinary Research Center for Construction and Building Materials, KFUPM, 31261 Dhahran, Saudi Arabia*

(*Received April 11, 2023, Revised December 31, 2023, Accepted January 3, 2024*)

Abstract. In current investigation, a novel beam finite element model is formulated to analyze the buckling and free vibration responses of functionally graded porous beams resting on Winkler-Pasternak elastic foundations. The novelty lies in the formulation of a simplified finite element model with only three degrees of freedom per node, integrating both C^0 and C^1 continuity requirements according to Lagrange and Hermite interpolations, respectively, in isoparametric coordinate while emphasizing the impact of z-coordinate-dependent porosity on vibration and buckling responses. The proposed model has been validated and demonstrating high accuracy when compared to previously published solutions. A detailed parametric examination is performed, highlighting the influence of porosity distribution, foundation parameters, slenderness ratio, and boundary conditions. Unlike existing numerical techniques, the proposed element achieves a high rate of convergence with reduced computational complexity. Additionally, the model's adaptability to various mechanical problems and structural geometries is showcased through the numerical evaluation of elastic foundations, with results in strong agreement with the theoretical formulation. In light of the findings, porosity significantly affects the mechanical integrity of FGP beams on elastic foundations, with the advanced beam element offering a stable, efficient model for future research and this in-depth investigation enriches porous structure simulations in a field with limited current research, necessitating additional exploration and investigation.

Keywords: beam finite element model; elastic stability; free vibration; porous functionally graded beam; Winkler-Pasternak elastic foundations

1. Introduction

In recent years, porous structures have garnered significant attention in various fields such as materials science, civil and mechanical engineering, and environmental engineering, due to their unique properties and potential applications. Porous structures are characterized by the insertion of interrelated voids or pores within a solid matrix, offering a variety of useful properties such as high surface area, low density, and excellent adsorption capabilities (Chen *et al*. 2015, Wu *et al*. 2018, Jamshidi *et al*. 2019, Rachedi *et al*. 2020, Fan *et al*. 2021, Xiao *et al*. 2021, Bashiri *et al*. 2021, Madenci 2021, Yaylaci *et al*. 2022a, Ozdemir and Yaylaci 2023). These characteristics render these materials highly favorable in multiple applications, such as filtrations, catalysis, energy storage, and even biomedical engineering. Investigating porous structures proves essential for knowledge of overall mechanical, thermal, and chemical attributes that ultimately determine their effectiveness in practical situations. Various methodologies have been proposed to examine porous structures, combining both experimental methods and computational approaches (Yaylaci 2016, Yaylaci *et al*. 2022d). Via optimum use of such techniques, researchers and professionals can get valuable information about the properties of porous materials and their impact within practical use.

However, structures rested on elastic foundations involve an intricate interaction between the structure and foundation layers (Zhang *et al*. 2015, Lee *et al*. 2015, Duc *et al*. 2015, Ghorbanpour *et al*. 2018, Yaylaci *et al*. 2021, Adiyaman *et al*. 2023, Yaylaci *et al*. 2022e, Yaylaci *et al*. 2022f, Assie *et al*. 2023, Mohamed *et al*. 2022). These interactions have an important influence on the mechanical behavior and performance of the structure. Elastic foundation models, including the Winkler and Pasternak models, are essential assets in numerous engineering fields over structural analysis including multiple layers. The Winkler elastic foundation is commonly simulated as a

*Corresponding author, Professor
E-mail: tou_abdel@yahoo.com

ISSN: 2005-307X (Print), 2092-6219 (Online)

fundamental model employing the spring concept in the vertical direction. In contrast, the Pasternak elastic foundation incorporates a shear layer. Both elastic foundation models serve as a pivotal factor in foundation design, to maintain a harmonious equilibrium balance among simplicity and accuracy. This balance is essential for the analysis and design of structures interacting with different foundation layers under various mechanical conditions. Porous beams resting on elastic foundations present an advanced research, combining the basic concepts of porous materials with the ever-present interaction amongst each other (Ahmed *et al*. 2019, Arefi and Zur 2020, Alnujaie *et al*. 2021, Al-Toki *et al*. 2022, Yaylaci *et al*. 2022b, Yaylaci 2022c, Oner *et al*. 2022, Esen *et al*. 2021c, Shanab *et al*. 2022, and Melaibari *et al*. 2022).

Among some applications in this field, Ait Atmane *et al*. (2015) proposed a refined shear beam theory to examine the mechanical behavior of functionally graded beams resting on elastic foundations. Chen *et al*. (2016) studied the effect of porosities on the mechanical response of metal foam beams under various dynamical loadings. Ebrahimi and Jafari (2016) investigated the vibrational behavior of beams in thermal environment with porosity by employing the Timoshenko beam theory and the semi-analytical differential transform method. Setoodeh and Rezaei (2017) proposed a closed-form solution to analyze the geometrically nonlinear free vibration response of functionally graded beams resting on nonlinear elastic foundations. Akbas (2017) studied the effect of porosities on the free vibration of functionally graded deep beams in the thermal environment. Avcar and Mohammed (2018) assessed the impact of elastic foundations on fundamental frequencies of functionally graded beams with different boundary conditions, utilizing the variable separation method. Liu *et al*. (2018) investigated size-dependent vibrational behaviors of porous functionally graded magneto-electro-viscoelastic nanobeams in a viscoelastic medium, using the nonlocal Timoshenko beam theory and the Kelvin-Voigt model. Al-shujairi and Mollamahmutoglu (2018) analyzed the impact of various parameters on the buckling and free vibration responses of sandwich nanobeams resting on elastic foundations by applying different higher-order shear theories under thermal loads. Fazzolari (2018) examined the free vibration and elastic stability of 3D functionally graded sandwich beams with various parameters resting on Winkler-Pasternak elastic foundations by using both Hamilton's Principle and the Ritz method. Al-Maliki *et al*. (2019) proposed a refined thick beam finite element to analyze the free vibration behavior of metal foam beams with symmetric and non-symmetric porosity distribution patterns. Jalaei and Civalek (2019) applied the Timoshenko beam theory to study advanced mechanical responses of functionally graded nanobeams including viscoelastic layer. Avcar (2019) conducted the free vibration response on functionally graded beams including the porosity within the assumption of Timoshenko beam theory and the separation of variables process. Ebrahimi and Dabbagh (2019) introduced an explicit finite element simulation for determining the fundamental frequencies of nanobeams with varying porosities. Jena *et al*. (2020) employed the Rayleigh-Ritz method with Navier solution to study the free vibration behavior of functionally graded porous beams rested on the Kerr foundation. Melaibari *et al*. (2020) explored the buckling behavior of advanced composite beams with axial loading, utilizing parabolic refined shear beam theory. Hamed *et al*. (2020) studied the effect of compressive force on the critical buckling loads and modes of sandwich composite laminated beams resting on Winkler and Pasternak elastic foundations, using unified higher-order shear beam theories, Hamilton's principle, and the differential quadrature numerical method to derive equilibrium equations. Uzun *et al*. (2020) explored Eringen's theory to investigate the free vibration behavior of functionally graded nanobeams resting on the Winkler elastic foundation. Akbas *et al*. (2020a) developed an efficient computational model to analyze the advanced vibration behavior of thick functionally graded porous beams subjected to dynamical sine pulse loadings, and considering the damping effect. Akbas *et al*. (2020b) performed a dynamic response of tri-layered composite thick beams with a porous layer resting on a viscoelastic foundation. Khoram *et al*. (2020) presented a refined technique to analyze the bending response of composite beams with bi-directional variations supported by two-parameter elastic foundations in magnetic field. Zhang *et al*. (2021) introduced an innovative computational technique to examine the vibrational behavior of porous beams on elastic foundations, reinforced by graphene platelets, and subjected to moving loads. Wang *et al*. (2021) analyzed the impact of the viscoelastic foundation and moving loads on the nonlinear vibration behavior of graphene oxide-reinforced curved beams based on the third order shear deformable beam theory with semi-analytical solutions. Ghandourah *et al*. (2021) analyzed the vibration response of porous functionally graded nanobeams based on the hypothesis of both Eringen's and Euler-Bernoulli beam theories. Huang and Tahouneh (2021) used the Timoshenko beam theory to investigate the free vibration analysis of nanobeams with porosity resting on two-parameter elastic foundations. Esen *et al*. (2021a) conducted an extensive simulation of both vibration and stability responses of nanobeams in both thermal and magnetic environments. Van Long *et al*. (2022) utilized the Timoshenko beam theory to examine the nonlinear static behavior of functionally graded beams with porosity, embedded in the elastic foundation. Jena *et al*. (2022) presented wavelet-based techniques for the vibration analysis of Euler-Bernoulli nanobeams on Winkler-Pasternak elastic foundations. Pham *et al*. (2022) formulated a finite element model to explore the vibration behavior of functionally graded porous curved beams in hygrothermal conditions using the k-order shear deformation beam theory and resting on elastic foundations. Ansari *et al*. (2022) examined free vibrations in Timoshenko beam-type structures under rapid heating using micropolar thermo-elasticity and a novel numerical approach. Babaei *et al* (2022) implemented the third-order beam theory and von Kármán nonlinearity to analyze the thermal stability of nano-composite beams with porosities resting on a nonlinear medium. Yaylaci *et al*. (2023) investigated both vibration and buckling of a cracked

functionally graded material beam using the finite element method (FEM) and multilayer perceptron (MLP), the obtained results show that crack location, material properties, slenderness ratio, and end supports affect the bending vibration and buckling properties. Fouaidi *et al*. (2023) modeled porous polymer composite beams on elastic foundations reinforced with graphene oxide powders using The Timoshenko beam theory. Fallah and Aghdam (2023) investigated the potential application of physics-informed neural networks to analyze the flexural and vibrational behavior of 3D functionally graded porous beams with material properties continuously varying in three dimensions. Turan *et al*. (2023) used Timoshenko beam theory for free vibration and buckling analysis of functionally graded porous beams under different boundary conditions by employing finite element (FEM) and artificial neural network (ANN) methods, using Ritz-based analytical solutions and Lagrange's principle. Results show compatibility with FEM and ANN, obtaining normalized fundamental frequencies and critical buckling loads. Xin and Kiani (2023) investigated the impact of various aspects on the free vibration analysis of sandwich beams with a metal foam core resting on elastic foundations. Nguyen *et al*. (2023) conducted a comprehensive computational analysis to examine and evaluate the mechanical features of porous beams lying on Winkler and Pasternak elastic foundations.

These aforementioned investigations focus on the Euler-Bernoulli and Timoshenko beam theories. The Euler-Bernoulli theory has limits and overestimates some beam's mechanical behavior because it assumes that transverse shear stresses and rotating inertia can be neglected. In particular cases, the need for advanced theories can occur. However, the Timoshenko's theory provides a constant estimation of shear stress and necessitates an appropriate shear correction factor. Furthermore, it is crucial to assess the suitability of its application for each beam context, especially when dealing with variable cross-sections or composite material properties where it might not exactly reflect the mechanical response of specific beam under given boundary conditions. To address those limitations, it is necessary to apply higher-order beam theories suitable for the beam structure, mechanical simulations, and computational efficiency and precision requirements. To attain the desired degree of precision in advanced beam simulations, it is possible to implement a variety of techniques for solving larger, more complex problems or performing a large number of simulations in a given amount of time. Advances in computational efficiency often involve an array of factors, including the choice of a suitable resolution method, the guarantee of stability and convergence, and the ease of straightforward implementation. Eventually, the finite element approach is recognized as a powerful and adaptable numerical technique that offers numerous advantages for advanced beam simulations, including flexibility, adaptively, accuracy, precision, robustness, and expandability, in comparison to these other advanced numerical procedures.

The current analysis investigates the features of functionally graded porous beams, evaluating potential applications in aeronautical, civil, and mechanical engineering to assist in the development of lighter and more durable structural systems. This study explores the elastic stability and vibration responses of various systems. The objective aims to enhance safety and efficiency. The result provides a new perspective on porosity within the field of materials science, which might inspire future progress in developing composites with specific attributes for particular purposes. The principal focus of this research is to develop and evaluate an advanced and effective beam element for estimating the buckling and free vibration characteristics of porous functionally graded beams supported by Winkler and Pasternak elastic foundations. In the scope of current research, an innovative beam element model is founded on the refined hyperbolic higher-order shear deformation theory to analyze porous beams resting on elastic foundations, offering high accuracy in assessing the elastic stability and free vibration behaviors. The proposed model integrates both Lagrange and Hermite interpolations to ensure the inter-element continuity requirements. The porosity is considered by symmetric and asymmetric distribution patterns in z-dependent coordinate, to enhance the comprehension of porous beam behavior. To highlight the developed model's efficiency and accuracy, an in-depth comparative examination is performed, assessing the obtained results with other established computational solutions. Considering multiple factors such as porosity distribution patterns, Winkler-Pasternak coefficients, aspect ratio, and boundary conditions, the current investigation conducts an extensive exploration for porous beams on elastic foundations. Hence, the present work reveals an important contribution by improving the strategy for establishing and improving beam concepts, especially for contexts where further study will be required and rather unexplored. This model not only advances the theoretical framework but also sets a new benchmark for practical applications in structural engineering.

2. Problem formulation

2.1 Characteristics of graded porous beams

A beam with graded porosity in z-dependent coordinate with length L and uniform section $b \times h$ (b is the width and h is the beam's thickness) supported on both Winkler and Pasternak elastic foundations is considered, as illustrated in Fig. 1. (x, y, z) present the Cartesian coordinates, at ($z = 0$) the plane (x, y) coincides with the middle layer of the porous beam. The functionally graded porous beam is loaded by an axially compressive force P_0 at its ends. The variation of the porosity is assumed smoothly in the z-dependent coordinate according to graded symmetric and asymmetric distribution patterns.

Metal foam is a material with characteristics that are homogeneous and tolerant, and it exhibits controlled porosity, allowing the material an array of features. The relatively stable microstructure, characterized by narrow reinforces and exceptional surface roughness, allows for flexible adaptation through the insertion of semiconductor

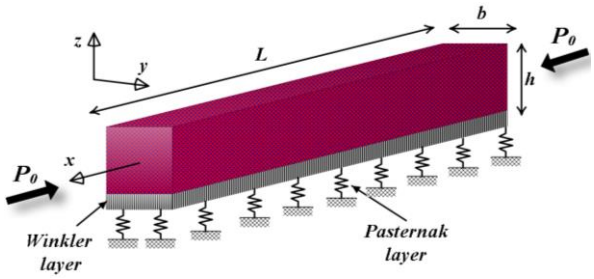

Fig. 1 Presentation on the geometry of porous beam resting on Winkler/Pasternak elastic foundations.

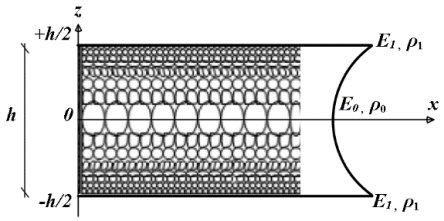

Fig. 2 Symmetric porosity distribution pattern

cells or adjustments in the basic structure of a metal alloy. Metal foam is provided to offer a reliable and adaptable foundation, which inspires innovation in an extensive spectrum of industries. This section examines the detailed aspects of metal foam, examining its structural properties, the potential for configuration, and its impact on material science and composite materials. The porous beams are designed to vary continuously and smoothly through the thickness gradient. The porosity allows for the inclusion of distribution patterns within the constituent properties of beams. To derive the effective properties of porous beams, two porosity distribution patterns are used. The Young's modulus, shear modulus, and mass density all vary across the thickness coordinate of porous beam, revealing symmetric and asymmetric porosity distribution patterns as shown in Figs. 2 and 3. These distribution patterns can be expressed mathematically using the following formula (Chen *et al*. 2016, Nguyen *et al*. 2023)

$$E(z)=E_1\left[1-e_0\cos\left(\frac{\pi z}{h}\right)\right];\ G(z)=G_1\left[1-e_0\cos\left(\frac{\pi z}{h}\right)\right]$$
$$\rho(z)=\rho_1\left[1-e_m\cos\left(\frac{\pi z}{h}\right)\right] \tag{1}$$

$$E(z)=E_1\left[1-e_0\cos\left(\frac{\pi z}{2h}+\frac{\pi}{4}\right)\right]$$
$$G(z)=G_1\left[1-e_0\cos\left(\frac{\pi z}{2h}+\frac{\pi}{4}\right)\right] \tag{2}$$
$$\rho(z)=\rho_1\left[1-e_m\cos\left(\frac{\pi z}{2h}+\frac{\pi}{4}\right)\right]$$

and

$$e_m=1-\sqrt{1-e_0} \tag{3}$$

Where (E_1, G_1 and ρ_1) and (E_0, G_0 and ρ_0) present the maximum and minimum Young's modulus, shear modulus, and mass density of porous beams, respectively. e_0 and e_m note the porosity coefficients of the relative material properties of porous beams.

2.2 The kinematics of the present formulation

The current theoretical investigation incorporates shear effects via a hyperbolic warping function of all displacement components throughout the beam's thickness, while obeying stress-free boundary requirements on both the upper and lower beam surfaces, eliminating the necessity for a shear correction coefficient. Furthermore, to deal with functionally graded porous beam problems, the accuracy, and efficacy of the computations that result from the present beam theory needed to be improved. The displacement field relations shown below can be obtained (Nguyen *et al*. 2023, Abdelbari *et al*. 2023, Melaibari *et al*. 2020)

$$u(x,z,t)=u_0(x,t)-z\frac{\partial w_0(x,t)}{\partial x}+f(z)\phi(x,t)$$
$$w(x,z,t)=w_0(x,t) \tag{4}$$

Where $u_0(x,t)$ is the axial displacement; $w_0(x,t)$ is the transverse displacements of a mid-line point of the beam; $\phi(x,t)$ is the rotation of the cross-section of the beam at the neutral axis due to transverse shear deformation. $f(z)$ presents the warping function, and characterizes the change in the transverse shear strains and shear stresses through the thickness, and expressed as follows (Belabed *et al*. 2021)

$$f(z)=\frac{\cosh\left(\frac{\pi}{2}\right)h^2\left(z\pi\cosh\left(\frac{\pi}{2}\right)-h\sinh\left(\frac{\pi z}{h}\right)\right)}{\frac{\pi}{2}\left(\cosh\left(\frac{\pi}{2}\right)-1\right)} \tag{5}$$

The strain field related to the displacement in Eq. (4) can be expressed as follows

$$\varepsilon_x=\frac{\partial u_0}{\partial x}-z\frac{\partial^2 w_0}{\partial x^2}+f(z)\frac{\partial\phi}{\partial x}$$
$$\gamma_{xz}=g(z)\phi \tag{6}$$

The first derivative of warping function is given as follows

$$g(z)=\frac{\partial f(z)}{\partial z} \tag{7}$$

By substituting Eq. (4) into Eqs. (6), the following strain displacement relations are obtained for the used refined shear deformation beam theory

$$\varepsilon_x=\varepsilon_x^0+zk_x+f(z)\eta_x \tag{8}$$

and

$$\varepsilon_x^0=\frac{\partial u_0}{\partial x},\ k_x=-\frac{\partial^2 w_0}{\partial x^2},\ \eta_x=\frac{\partial\varphi_x}{\partial x},\ \gamma_{xz}^0=\phi \tag{9}$$

2.3 Constitutive relations

The linear constitutive relations of an FGP beam can be expressed as follows (Hamed *et al*. 2020, Esen *et al*. 2021a,b,c)

$$\begin{Bmatrix}\sigma_x\\ \tau_{xz}\end{Bmatrix}=\begin{bmatrix}Q_{11} & 0\\ 0 & Q_{44}\end{bmatrix}\begin{Bmatrix}\varepsilon_x\\ \gamma_{xz}\end{Bmatrix} \tag{10}$$

where σ_x and τ_{xz} are the stress components and Q_{ij} represent the rigidity parameters associated with the material property constants in well-known engineering applications

$$Q_{11}=E(z),\ Q_{44}=G(z)=\frac{E(z)}{2(1+\nu)} \tag{11}$$

In this study, *E(z)* and *G(z)* are the Young's, the shear modulus, respectively, and suppose that they are *z*-dependent. The Poisson's ratio is denoted by υ and is assumed constant.

3. Weak variational formulation

Based on Hamilton's principle, the governing differential equations are consistently derived to define the problem. This principle is elaborated in an extended variational version as described below (Madenci *et al*. 2021, Fazzolari 2018, Avcar 2019, Jena *et al*. 2020)

$$\int_{t_1}^{t_2}\delta\left(K-\left(U+U_f+V\right)\right)dt=0 \tag{12}$$

where $(U+U_f)$ is the sum of the strain and elastic foundation energies of the porous beam, and *V* presents the potential energy of the applied compression load, and *K* represents the kinetic energy. The variation of strain energy of the porous beam is given by

$$\begin{aligned}\delta U&=\int_V\left(\sigma_x\delta\varepsilon_x+\tau_{xz}\delta\gamma_{xz}\right)dV\\&=\int_A\left(N_x\delta\varepsilon_x^0+M_x\delta k_x+S_x\delta\eta_x+Q_{xz}\delta\gamma_{xz}^0\right)dA\end{aligned} \tag{13}$$

where *A* is the uniform cross-section. The stress resultants N_x, M_x, S_x and Q_{xz} are given as

$$\left(N_x,M_x,S_x\right)=\int_{-h/2}^{h/2}\sigma_x\left(1,z,f\right)dz, \tag{14a}$$

and

$$\left(N_x,M_x,S_x\right)=\int_{-h/2}^{h/2}\sigma_x\left(1,z,f\right)dz, \tag{14b}$$

where *h/2* and *-h/2* are the coordinate of the top and bottom surfaces of the porous beam, respectively. By replacing Eqs. (8) and (11) into Eqs. (14), and the stress resultant expressions are given as

$$\begin{aligned}N_x&=A_{11}\varepsilon_x^0+B_{11}k_x+B_{11}^s\eta_x\\M_x&=B_{11}\varepsilon_x^0+D_{11}k_x+H_{11}^s\eta_x\\S_x&=B_{11}^s\varepsilon_x^0+H_{11}^sk_x+D_{11}^s\eta_x\\Q_{xy}&=A_{44}^s\gamma_{xz}^0\end{aligned} \tag{15}$$

where the stiffness coefficients are defined as:

$$\begin{aligned}\left(A_{11},B_{11},D_{11},B_{11}^s,H_{11}^s,D_{11}^s\right)&=\int_{-h/2}^{h/2}\left(1,z,z^2,f,zf,f^2\right)Q_{11}dz,\\A_{55}^s&=\int_{-h/2}^{h/2}g(z)^2Q_{55}dz\end{aligned} \tag{16}$$

The variation of the foundation energy including the Winkler and Pasternak parameters can be given by (Ait Atmane *et al*. 2015, Al-shujairi *et al*. 2018, Alnujaie *et al*. 2021, Ebrahimi *et al*. 2021)

$$\delta U_f=\frac{1}{2}\int_V\left[k_W w\delta w+k_P\left(\frac{\partial w}{\partial x}\right)\left(\frac{\partial\delta w}{\partial x}\right)\right]dV \tag{17}$$

where k_W and k_P represent the Winkler and Pasternak elastic foundation coefficients, respectively.

The variation of the potential energy of the applied compression load can be given by

$$\delta V=\frac{1}{2}\int_V\left[P_{0x}\left(\frac{\delta\partial w}{\partial x}\right)\left(\frac{\partial w}{\partial x}\right)\right]dV \tag{18}$$

The variation of the kinetic energy of the mass system can be written as

$$\begin{aligned}\delta K&=\int_V\left[\ddot{u}\delta u+\ddot{w}\delta w\right]\rho(z)dV\\&=\int_A\left\{\left(I_1\ddot{u}_0\delta u_0+I_1\ddot{w}_0\delta w_0\right)-I_2\left(\ddot{u}_0\frac{\partial\delta w_0}{\partial x}+\frac{\partial\ddot{w}_0}{\partial x}\delta u_0\right)\right.\\&+I_3\left(\frac{\partial\ddot{w}_0}{\partial x}\frac{\partial\delta w_0}{\partial x}\right)+I_4\left(\ddot{\phi}\delta u_0+\ddot{u}_0\delta\phi\right)\\&\left.-I_5\left(\ddot{\phi}\frac{\partial\delta w_0}{\partial x}+\frac{\partial\ddot{w}_0}{\partial x}\delta\phi\right)+I_6\left(\ddot{\phi}\delta\phi\right)\right\}dA\end{aligned} \tag{19}$$

$\rho(z)$ is the mass density; and $(I_1, I_2, I_3, I_4, I_5, I_6)$ are mass inertias defined by

$$\left(I_1,I_2,I_3,I_4,I_5,I_6\right)=\int_{-h/2}^{h/2}\rho(z)\left(1,z,z?\ f,z\ f,f^2\right)dz \tag{20}$$

Inserting Eqs. (13), (17), (18), and (19) into Eq. (12), taking the variations of δU, δU_f, δV and δK, integrating by parts, and setting each of the virtual displacements of δu_0, δw_0 and $\delta\phi$, the following weak version of governing equations of the porous beam can be expressed as

$$\begin{aligned}&\int_L\left[\left\langle\delta\varepsilon_x^0\right\rangle A_{11}\left\{\varepsilon_x^0\right\}+\left\langle\delta\varepsilon_x^0\right\rangle B_{11}\left\{k_x\right\}+\left\langle\delta\varepsilon_x^0\right\rangle B_{11}^s\left\{\eta_x\right\}\right.\\&+\left\langle\delta k_x\right\rangle B_{11}\left\{\varepsilon_x^0\right\}+\left\langle\delta k_x\right\rangle D_{11}\left\{k_x\right\}+\left\langle\delta k_x\right\rangle H_{11}^s\left\{\eta_x\right\}\\&+\left\langle\delta\eta_x\right\rangle B_{11}\left\{\varepsilon_x^0\right\}+\left\langle\delta\eta_x\right\rangle D_{11}\left\{k_x\right\}+\left\langle\delta\eta_x\right\rangle H_{11}^s\left\{\eta_x\right\}\\&+\left\langle\delta\gamma_{xz}^0\right\rangle A_{44}^s\delta\gamma_{xz}^0+k_w\left\langle\delta w\right\rangle\left\{w\right\}+k_P\left\langle\frac{\delta\partial w}{\partial x}\right\rangle\left\{\frac{\partial w}{\partial x}\right\}\\&+P_0\left\langle\frac{\delta\partial w}{\partial x}\right\rangle\left\{\frac{\partial w}{\partial x}\right\}+\left\langle\delta u_0\right\rangle I_1\left\langle\ddot{u}_0\right\rangle+\left\langle\delta w_0\right\rangle I_1\left\langle\ddot{w}_0\right\rangle\\&-\left\langle\delta w_0\right\rangle I_2\left\langle\frac{\partial\ddot{u}_0}{\partial x}\right\rangle-\left\langle\delta u_0\right\rangle I_2\left\langle\frac{\partial\ddot{w}_0}{\partial x}\right\rangle+\left\langle\delta w_0\right\rangle I_3\left\langle\frac{\partial^2\ddot{w}_0}{\partial x^2}\right\rangle\\&+\left\langle\delta u_0\right\rangle I_4\left\langle\ddot{\phi}\right\rangle+\left\langle\delta\phi\right\rangle I_4\left\langle\ddot{u}_0\right\rangle-\left\langle\delta w_0\right\rangle I_5\left\langle\frac{\partial\ddot{\phi}}{\partial x}\right\rangle\\&\left.-\left\langle\delta\phi\right\rangle I_5\left\langle\frac{\partial\ddot{w}_0}{\partial x}\right\rangle+\left\langle\delta\phi\right\rangle I_6\left\langle\ddot{\phi}\right\rangle\right]dx=0\end{aligned} \tag{21}$$

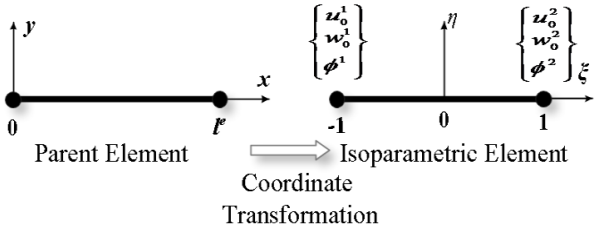

Fig. 4 The geometrical transformation of the present Beam element.

4. Finite element formulation

The beam is discretized into a series of elementary lengths denoted by l_e. Fig. 4 depicts a two-node beam element with three degrees of freedom associated at each node. The following relation presents the mapping transformation from the physical coordinate to a reference or parametrical coordinate

$$x(\xi)=\frac{1+\xi}{2}l_e \tag{22}$$

where

$$dx=J\cdot d\xi,\quad \frac{\partial f}{\partial x}=J^{-1}\cdot\frac{\partial f}{\partial \zeta},\quad J=\frac{l_e}{2}\quad J^{-1}=\frac{1}{J}$$
$$\int_0^L f(x)dx=\int_{-1}^{1} f(x(\zeta))\cdot J\cdot d\zeta \tag{23}$$

and J is the Jacobian operator.

For the present two-node beam element is formulated in the isoparametric coordinate and the shape functions N_i and H_i are expressed as (Zienkiewicz *et al*. 2005, Dhatt *et al*. 2012)

$$\{N_i\}=\begin{Bmatrix}N_1\\N_2\end{Bmatrix}=\begin{Bmatrix}\frac{1}{2}(1-\xi)\\\frac{1}{2}(1+\xi)\end{Bmatrix}$$
$$\{H_i\}=\begin{Bmatrix}H_1\\H_2\\H_3\\H_4\end{Bmatrix}=\frac{1}{4}\begin{Bmatrix}2-3\xi+\xi^2\\1-\xi-\xi^2+\xi^3\\2+3\xi-\xi^2\\-1-\xi+\xi^2+\xi^3\end{Bmatrix} \tag{24}$$

The unknown problem variables u_0 and ϕ approximated using C^0 continuity with the Lagrange interpolation function (N), whereas the unknown w_0 has been approximated using the C^1 continuity according to the Hermite cubic interpolation function (H).

The unknown displacements for the present beam element can be expressed as (Zienkiewicz *et al*. 2005, Dhatt *et al*. 2012)

$$u_0(\xi)=\sum_{i=1}^{2}N_i(\xi)u_0^i$$
$$\phi(\xi)=\sum_{i=1}^{2}N_i(\xi)\phi^i \tag{25}$$
$$w_0(\xi)=\sum_{i=1}^{4}H_i(\xi)w_0^i$$

where

$$u_0^e=\left\langle u_0^{(1)};\quad u_0^{(2)}\right\rangle^T$$
$$w_0^e=\left\langle w_0^{(1)}\quad w_{0,x}^{(1)};\quad w_0^{(2)}\quad w_{0,x}^{(2)}\right\rangle^T \tag{26}$$
$$\phi^e=\left\langle \phi^{(1)};\quad \phi^{(2)}\right\rangle^T$$

Hence, the strain-displacement relationships are derived as

$$\begin{aligned}\{\varepsilon_x^0\}&=[B]_m\{u_0^i\}\\\{k_x\}&=[B]_f\{w_0^i\}\\\{\eta_x\}&=[B]_s\{\varphi_x^i\}\\\{\gamma_{xz}^0\}&=[\overline{B}]_s\{\varphi_x^i\}\end{aligned} \tag{27}$$

The differential operator $[B]$ presents the strain-displacement derivative matrix, $[B]_m$, $[B]_f$, $[B]_s$, $[\overline{B}]_s$ $[B]_w$ and $[B]_0$ are the related membrane, bending, shear, higher-order shear, Winkler foundation, and both geometric and Pasternak foundation derivative operator matrices expressed as

$$\begin{aligned}[B]_m&=\sum_1^2\langle N_1\quad 0\quad 0\quad 0;\quad N_2\quad 0\quad 0\quad 0\rangle_i;\\[B]_f&=\sum_1^2\langle 0\quad 0\quad -H_{1,xx}\quad -H_{1,xx};\quad 0\quad 0\quad -H_{2,xx}\quad -H_{2,xx}\rangle_i;\\[B]_s&=\sum_1^2\langle 0\quad N_{1,x}\quad 0\quad 0;\quad 0\quad N_{2,x}\quad 0\quad 0\rangle_i;\\[\overline{B}]_s&=\sum_1^2\langle 0\quad N_1\quad 0\quad 0;\quad 0\quad N_2\quad 0\quad 0\rangle_i;\\[B]_w&=\sum_1^2\langle 0\quad 0\quad H_1\quad 0;\quad 0\quad 0\quad H_2\quad 0\rangle;\\[B]_0&=\sum_1^2\langle 0\quad 0\quad H_{1,x}\quad 0;\quad 0\quad 0\quad H_{2,x}\quad 0\rangle;\end{aligned} \tag{28}$$

Substituting Eq. (28) into Eq. (21) yields the nodal contributions to the element stiffness, geometric and mass matrices and takes the form:

$$\begin{aligned}&\langle\delta u_i\rangle\Big[\int_{-1}^{1}\Big(B_m^TA_{11}B_m+B_m^TB_{11}B_b+B_m^TB_{11}^sB_s+B_s^TB_{11}B_m\\&+B_b^TD_{11}B_b+B_b^TH_{11}^sB_s+B_s^TB_{11}B_m+B_s^TD_{11}B_b+B_s^TH_{11}^sB_s\\&+\overline{B}_s^TA_{44}^s\overline{B}_s+k_wB_W^TB_W+k_pB_0^TB_0+P_0B_0^TB_0+N^TI_1N\\&+H^TI_1H-H^TI_2N_{,x}-N^TI_2H_{,x}+H^TI_3H_{,xx}+N^TI_4N\\&+N^TI_4N-H^TI_5N_{,x}-N^TI_5H_{,x}+N^TI_6N\Big)Jd\xi\Big]\{u_i\}=0\end{aligned} \tag{29}$$

Eq. (29) can be reduced to conduct buckling eigenvalue analysis

$$\left([K]_g-P_0[G]_g\right)\{u_i\}=0 \tag{30}$$

After rewriting Eq. (29), the free vibration eigenvalue analysis is obtained in the form

$$\left([K]_g-\omega^2[M]_g\right)\{u_i\}=0 \tag{31}$$

where P_0 and ω present the critical buckling load and angular frequency respectively.

The global form of the stiffness, geometric and mass matrices are given by

$$\begin{aligned}[K]_g=\sum_e\big([K]_m+[K]_{mb}+[K]_{ms}+[K]_{bm}+[K]_b+[K]_{bs}\\+[K]_{sm}+[K]_{sb}+[K]_s+[\overline{K}]_s+[K]_W+[K]_P\big)\end{aligned} \tag{32a}$$

Table 1 Material properties used for porous beams

Properties	E_1 (GPa)	υ	ρ_1 (kg/m^3)
open-cell steel foam	200	0.3	7850

Table 2 Boundary conditions used in the present analysis

BCs	*x=0*	*x=L*
Simply-Supported (SS).	$u_0 = w_0 = 0; \phi_0 \neq 0$	$u_0 \neq \phi_0 \neq 0; w_0 = 0$
Clamped-Clamped (CC).	$u_0 = w_0 = \phi_0 = 0$	$u_0 = w_0 = \phi_0 = 0$
Clamped-free (CF).	$u_0 = w_0 = \phi_0 = 0$	$u_0 \neq w_0 \neq \phi_0 \neq 0$

$$[G]_g = \sum_e [K]_0 \tag{32b}$$

$$[M]_g = \sum_e \left([M]_m + [M]_b + [M]^1_{bm} + [M]^1_{mb} + [M]^2_b + [M]_{bs} + [M]_{sm} + [M]^1_{bs} + [M]^1_{sb} + [M]_s\right) \tag{32c}$$

These matrices are assembled by the element stiffness matrix, the element geometric matrix, and the element mass matrix, in which, they are evaluated numerically by using the Gauss quadrature rule and are provided in Appendix A.

5. Numerical results and discussion

In this part, the investigation of free vibration and buckling characteristics of functionally graded porous (FGP) beams resting on Winkler and Pasternak elastic foundations is conducted, while the material properties employed in this research are outlined in Table 1 for reference (Chen *et al*. 2016, Nguyen *et al* .2023):

The analysis of buckling and vibrational responses of functionally graded porous beams resting on Winkler and Pasternak elastic foundations examines the influence of porosity distribution patterns, Winkler and Pasternak foundation parameters, and various boundary conditions. Table 2 lists the kinetic boundary conditions of three used boundary conditions, namely clamped-clamped (CC), simply supported (SS), and clamped-free (CF). The non-dimensional results are presented in a normalized formula (Chen *et al*. 2016, Nguyen *et al*. 2023)

$$\hat{\omega} = \omega L \sqrt{\frac{\rho_1 (1-\upsilon^2)}{E_1}} \;;\; \hat{P}_{cr} = P_{cr} \frac{2(1-\upsilon^2)}{E_1 h};$$
$$\overline{\omega} = \sqrt[4]{\frac{\rho_1 A L^4 \omega^2}{E_1 I}} \;;\; \overline{P}_{cr} = P_{cr} \frac{L^2}{E_1 I}; \tag{33}$$
$$K_W = \frac{k_W L^4}{E_1 I}; \quad K_P = \frac{k_P L^2}{E_1 I}$$

where A and I are the cross-section and inertia of the FGP beam, respectively, as the following expression

$$A = bh \;;\; I = \frac{bh^3}{12} \tag{34}$$

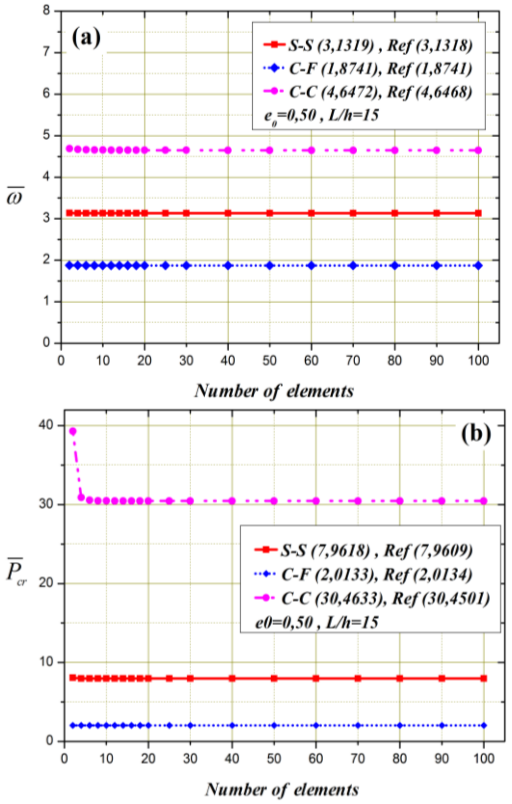

Fig. 5 Comparison and convergence of frequencies (a) and critical buckling load (b) as a function of mesh discretization of porous beams with CC , SS, and CF boundary conditions (e_0=*0.50* and *L/h=15*)

5.1 Convergence analysis

This section presents the results obtained from specified tests in the reference to evaluate the performance, accuracy, and convergence of the beam element developed in the current study. The analysis includes the porosity across the thickness. This section focuses on the vibration and buckling problems that are specifically associated with beams that have been discretized employing two-node finite beam elements. These tests are used to evaluate the formulation, demonstrate the convergence rate and accuracy dependent on the number of elements, and compare the performance attained when discretizing porous beams, among additional objectives. Therefore, the analysis also includes porous beams and various boundary conditions, such as fixed free edges, and simple supports. Fig. 5 illustrates the convergence curves for both fundamental frequencies and the critical buckling load, as a function of the number of elements. Nguyen *et al*. (2023) proposed the reference solution using third-order beam theory. The approach using finite elements exhibited a rapid and monotonic convergence towards the reference solution. Both case studies provide excellent results even with a limited number of elements. The convergence rate is fast and stable. Shear locking did not occur in this test example. Both mechanical behaviors well simulated the shear effects. The test is highlighted by the excellent performance of this element, especially due to the inclusion of porosity.

Table 3 Comparisons of the non-dimensional frequency of Simply Supported isotropic beams with various slenderness ratios and Winkler-Pasternak elastic foundation parameters

L/h	K_W	K_P	Theories				
			Present	Nguyen *et al.* (2023)	Chen *et al.* (2004)	Ying *et al.* (2008)	Ait Atmane *et al.* (2015)
5	0	0	3.04546	3.04541	3.04799	3.06373	3.04842
		π^2	3.66712	3.66710	3.65802	3.66645	3.65989
		2.5 π^2	4.23951	4.23950	4.21834	4.22319	4.22492
	10^2	0	3.67984	3.67981	3.67050	3.67882	3.67243
		π^2	4.08392	4.08390	4.06636	4.07200	4.07127
		2.5 π^2	4.52796	4.52795	4.49914	4.50278	4.50972
	10^4	0	7.37662*	7.37658	7.34081	7.34081	7.55257
		π^2	7.37662*	7.37658	7.34095	7.34095	7.55257
		2.5 π^2	7.37662*	7.37658	7.34116	7.34116	7.55257
15	0	0	3.12992	3.12991	3.13025	3.13227	3.13093
		π^2	3.72741	3.72740	3.72657	3.72775	3.72700
		2.5 π^2	4.28973	4.28972	4.28809	4.28886	4.28845
	10^2	0	3.73981	3.73980	3.73895	3.74012	3.73937
		π^2	4.13615	4.13615	4.13472	4.13558	4.13508
		2.5 π^2	4.57546	4.57546	4.57347	4.57410	4.57383
	10^4	0	10.01902**	10.01502	9.99582	9.99583	10.00663
		π^2	10.04310**	10.03909	10.01970	10.01971	10.03065
		2.5 π^2	10.07889**	10.07487	10.05519	10.05520	10.06635
120	0	0	3.14141	3.14141	3.14143	3.14145	3.14214
		π^2	3.73587	3.73587	3.73588	3.73587	3.73629
		2.5 π^2	4.29690	4.29690	4.29687	4.29689	4.29716
	10^2	0	3.74823	3.74823	3.74823	3.74823	3.74864
		π^2	4.14358	4.14358	4.14356	4.14357	4.14388
		2.5 π^2	4.58229	4.58229	4.58227	4.58227	4.58249
	10^4	0	10.02412	10.02412	10.02403	10.02403	10.02405
		π^2	10.04821	10.04821	10.04813	10.04812	10.04814
		2.5 π^2	10.08402	10.08402	10.08394	10.08393	10.08395

* Obtained results are given for *L/h*=10.
** Obtained results are given for *L/h*=20

5.2 Results of free vibration analysis

The first example focuses to examine the accuracy and validity of the current beam element. Table 3 represents the obtained non-dimensional fundamental frequencies of simply supported isotropic beams with different slenderness ratios and both Winkler and Pasternak elastic foundation parameters. The obtained results are compared with those from other theories, this includes Nguyen *et al*. (2023)'s parabolic shear deformation beam theory (PSDBT) using the Legendre-Ritz procedure, Ait Atmane *et al*. (2015)'s hyperbolic Quasi-3D shear deformation beam theory via an analytical solution, Ying *et al*. (2008)'s 2D elasticity solution employing the state space method, Chen *et al*. (2004)'s 2D elasticity solution of using the differential quadrature method. According to this comparison, the proposed beam element is in excellent accord with the reference solutions. The obtained results validate and prove the accuracy and performance of the used shear deformation beam theory and the current finite element formulation. The Winkler-Pasternak model of elastic foundations uses two models: the Winkler coefficient, which represents the foundation's vertical stiffness, and the Pasternak coefficient, which accounts for shear deformation and horizontal shear resistance. Both models are crucial in analyzing the free vibration of beams on these foundations. A higher Winkler coefficient leads to stiffer foundations, increasing fundamental frequencies. The Pasternak model, however, provides a more accurate depiction of foundation behavior, especially in shear deformation situations.

The following example has been performed for functionally graded porous beams without elastic foundations and different boundary conditions and slenderness ratios are considered. For both used porosity distribution patterns, this example analyzes the formulated element's accuracy and efficiency for FG beams in the presence of porosity (*e0=0.5*). Table 4 provides a comparison of obtained first non-dimensional fundamental frequency with existing results from reference. To evaluate the precision of the developed beam element, the obtained results are compared to those given by the Legendre-Ritz solutions of Nguyen *et al*. (2023) by employing a higher-order shear deformation beam theory and Nguyen *et al*. (2022) using a refined shear deformation beam theory and Ritz procedure, and Timoshenko beam theory with discrete singular convolution method from Gao *et al*. (2019), respectively. It should be noted that the given Ritz method is based on Lagrange's equations and resolved by using admissible functions. The discrete singular convolution approach is founded on the hybrid Chebyshev surrogate

Table 4 The comparison of the non-dimensional frequency $\hat{\omega}$ of porous functionally graded beams with various boundary conditions and slenderness ratios *(e_0=0.5*)

BCs	*L/h*	Porosity Pattern	Theories				
			Present	Nguyen *et al*. (2023)	Nguyen *et al*. (2022)	Chen *et al*. (2016)	Gao *et al*. (2019)
S-S	10	Porosity I	0.2794	0.2791	0.2791	0.2798	0.2798
		Porosity II	0.2548	0.2549	/	0.2599	0.2599
	20	Porosity I	0.1421	0.1421	0.1421	0.1422	0.1422
		Porosity II	0.1292	0.1293	/	0.1318	0.1320
C-F	10	Porosity I	0.1007	0.1007	0.1007	0.1008	0.1008
		Porosity II	0.0917	0.0917	/	0.0917	0.0917
	20	Porosity I	0.0508	0.0508	0.0508	0.0508	0.0508
		Porosity II	0.0462	0.0462	/	0.0462	0.0462
C-C	10	Porosity I	0.5925	0.5900	0.5908	0.5944	0.5945
		Porosity II	0.5476	0.5476	/	0.5475	0.5475
	20	Porosity I	0.3163	0.3159	0.3160	0.3166	0.3166
		Porosity II	0.2888	0.2888	/	0.2888	0.2888

Table 5 The comparison of the non-dimensional frequency $\overline{\omega}$ of Simply-Supported porous functionally graded beams with various distribution patterns and Winkler-Pasternak elastic foundation coefficients (*e0*=0.5 and *L/h*=15)

K_P	Porosity Pattern	Theories	K_W				
			0	10	50	100	500
0	Porosity I	Nguyen *et al*. (2023)	3.1318	3.2271	3.5422	3.8454	5.1591
		Present	3.1319	3.2271	3.5422	3.8454	5.1591
	Porosity II	Nguyen *et al*. (2023)	2.9884	3.0970	3.4458	3.7710	5.1291
		Present	2.9879	3.0966	3.4454	3.7706	5.1286
π^2	Porosity I	Nguyen *et al*. (2023)	3.8313	3.8846	4.0785	4.2875	5.3637
		Present	3.8314	3.8847	4.0785	4.2875	5.3637
	Porosity II	Nguyen *et al*. (2023)	3.7561	3.8126	4.0166	4.2345	5.3372
		Present	3.7557	3.8122	4.0162	4.2341	5.3366
2.5 π^2	Porosity I	Nguyen *et al*. (2023)	4.4563	4.4905	4.6200	4.7680	5.6327
		Present	4.4564	4.4906	4.6201	4.7680	5.6327
	Porosity II	Nguyen *et al*. (2023)	4.4093	4.4446	4.5780	4.7298	5.6098
		Present	4.4089	4.4442	4.5775	4.7293	5.6092
5 π^2	Porosity I	Nguyen *et al*. (2023)	5.1300	5.1525	5.2398	5.3430	6.0101
		Present	5.1300	5.1525	5.2398	5.3431	6.0101
	Porosity II	Nguyen *et al*. (2023)	5.0995	5.1224	5.2112	5.3162	5.9914
		Present	5.0989	5.1219	5.2106	5.3156	5.9907

model to approximate the governing equations. Once again, the precision and accuracy of derived non-dimensional fundamental frequencies have been confirmed for all imposed boundary conditions, showing perfect agreement with the results obtained from other advanced numerical methods. For both porosity distribution patterns, this implies that obtained results have an optimal rate of validity and confirms the excellent performance of the formulated beam element dealing with free vibration problems of porous beams. Various established computational approaches such as the discrete singular convolution (DSC), Ritz method, and Legendre-Ritz methods exhibit limits once analyzing the free vibration response of porous beams. Aside from being marginally applicable and the requiring computational cost, the DSC method may pose difficulties related to issues with numerical implementation and stability. Furthermore, the Ritz method frequently necessitates selecting proper trial functions, and unfavorable for numerical perspective and maintaining slower convergence rates. As well as, the necessity of the Legendre-Ritz method for proper orthogonal polynomials suggests challenge in the use and numerical implementation, especially for atypical boundary conditions or irregular geometries. The porosity distribution pattern in beams, whether symmetric or asymmetric, significantly influences fundamental frequencies. The symmetric pattern balances stiffness and density, resulting in a maximum magnitude of fundamental frequencies. Conversely, the asymmetric pattern reduces stiffness and density, resulting in lower frequency magnitudes. Therefore, an appropriate distribution pattern must be considered with specific porosity distribution patterns and material characteristics to

Table 6 Comparisons of the non-dimensional frequency $\overline{\omega}$ of Clamped-Clamped porous functionally graded beams with various distribution patterns and Winkler-Pasternak elastic foundation parameters (*e0*=0.5 and *L/h*=15)

K_P	Porosity Pattern	Theories	K_W				
			0	10	50	100	500
0	Porosity I	Nguyen *et al*. (2023)	4.6468	4.6770	4.7923	4.9256	5.7303
		Present	4.6472	4.6774	4.7926	4.9260	5.7305
	Porosity II	Nguyen *et al*. (2023)	4.4498	4.4841	4.6141	4.7625	5.6292
		Present	4.4482	4.4825	4.6127	4.7613	5.6284
π^2	Porosity I	Nguyen *et al*. (2023)	4.9700	4.9948	5.0902	5.2025	5.9127
		Present	4.9703	4.9950	5.0905	5.2027	5.9128
	Porosity II	Nguyen *et al*. (2023)	4.8129	4.8402	4.9447	5.0667	5.8217
		Present	4.8114	4.8387	4.9433	5.0654	5.8209
2.5 π^2	Porosity I	Nguyen *et al*. (2023)	5.3541	5.3739	5.4511	5.5432	6.1535
		Present	5.3541	5.3740	5.4511	5.5433	6.1535
	Porosity II	Nguyen *et al*. (2023)	5.2308	5.2521	5.3346	5.4327	6.0737
		Present	5.2293	5.2506	5.3332	5.4313	6.0727
5 π^2	Porosity I	Nguyen *et al*. (2023)	5.8435	5.8588	5.9187	5.9912	6.4937
		Present	5.8433	5.8586	5.9185	5.9910	6.4935
	Porosity II	Nguyen *et al*. (2023)	5.7500	5.7660	5.8288	5.9046	6.4262
		Present	5.7482	5.7642	5.8271	5.9030	6.4249

Table 7 Comparisons of the non-dimensional frequency $\overline{\omega}$ of Clamped-Free porous functionally graded beams with various distribution patterns and Winkler-Pasternak elastic foundation parameters (*e0*=0.5 and *L/h*=15)

K_P	Porosity Pattern	Theories	K_W				
			0	10	50	100	500
0	Porosity I	Nguyen *et al*. (2023)	1.8741	2.2272	2.9298	3.4088	5.0016
		Present	1.8741	2.2272	2.9298	3.4088	5.0016
	Porosity II	Nguyen *et al*. (2023)	1.7872	2.1773	2.9085	3.3954	4.9974
		Present	1.7872	2.1773	2.9084	3.3954	4.9974
π^2	Porosity I	Nguyen *et al*. (2023)	2.7604	2.8959	3.3059	3.6670	5.0912
		Present	2.7601	2.8957	3.3057	3.6669	5.0911
	Porosity II	Nguyen *et al*. (2023)	2.7229	2.8636	3.2843	3.6513	5.0854
		Present	2.7225	2.8633	3.2841	3.6511	5.0854
2.5 π^2	Porosity I	Nguyen *et al*. (2023)	3.2665	3.3512	3.6384	3.9221	5.1939
		Present	3.2660	3.3508	3.6380	3.9218	5.1938
	Porosity II	Nguyen *et al*. (2023)	3.2357	3.3228	3.6163	3.9045	5.1864
		Present	3.2350	3.3221	3.6158	3.9041	5.1863
5 π^2	Porosity I	Nguyen *et al*. (2023)	3.7570	3.8136	4.0180	4.2361	5.3401
		Present	3.7562	3.8128	4.0173	4.2356	5.3398
	Porosity II	Nguyen *et al*. (2023)	3.7322	3.7899	3.9978	4.2190	5.3316
		Present	3.7312	3.7889	3.9969	4.2182	5.3312

investigate the porous beams' free vibration behavior.

The next example is performed for FGP beams resting on both Winkler and Pasternak elastic foundations with simply supported boundary conditions. Table 5 compares the obtained non-dimensional fundamental frequencies with those given by Nguyen *et al*. (2023). This Table indicates a high rate of agreement is observed, confirming both accuracy and efficiently of the formulated finite element beam model. It is observed also that both elastic foundation coefficients contribute in rising the fundamental frequency of porous beams. The Winkler elastic foundation presents impact that is more significant on the obtained results. Two porosity patterns: Symmetrical and asymmetrical distributions have a variable influence, the symmetric distribution across the beam's thickness provide an excellent balance between the derived rigidity and density, resulting in reduced obtained frequencies magnitudes compared to those given by asymmetric distribution that introduces additional non uniform material characteristics. In light of this example, the porosity distribution and elastic foundation parameter merit further consideration regarding the free vibration behavior of porous beams including simply supported edges and must be explored to other case studies. On the inspiration of Tables 5 and 6, the influence

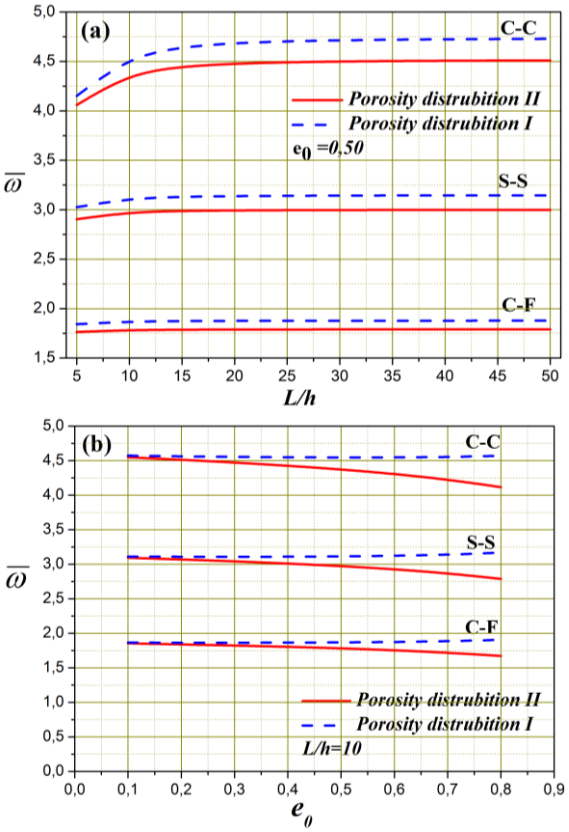

Fig. 6 Variation of the non-dimensional fundamental frequency of porous beams without elastic foundations as a function of slenderness ratios (a) and porosity parameters (b) for various boundary conditions

of Winkler and Pasternak elastic foundation coefficients and porosity distribution patterns on the first non-dimensional fundamental frequencies of FGP beams has been examined. Clamped-Clamped and Clamped-Free, respectively, have been considered as boundary conditions. These examples provided additional validation to confirm the accuracy of the obtained results. Nguyen *et al*. (2023) used the Legendre-Ritz method for solving the free vibration problem with higher-order shear deformation theory and yielded outcomes that closely resembled those obtained using the current beam finite element formulation. The developed element effectively observed the same effect without numerical issues, serving as a basis for future research on porous beams resting on Winkler and Pasternak elastic foundations. Results highlighted that Winkler and Pasternak's coefficients have a more significant effect than porosity distribution patterns, especially for rigid elastic foundations. While both elastic foundation coefficients increase, non-dimensional fundamental frequencies increase too, and for higher Pasternak coefficients, the difference between the presented fundamental frequencies seem to be reduced. For visual inspection of the multiple impact of slenderness ratio, porosity, and elastic foundations on the non-dimensional frequency, Figs. 6-9 illustrate the variation of non-dimensional frequencies of porous beams with CC, SS, and CF boundary conditions. It is observed that both slenderness ration and porosity insertion influence the

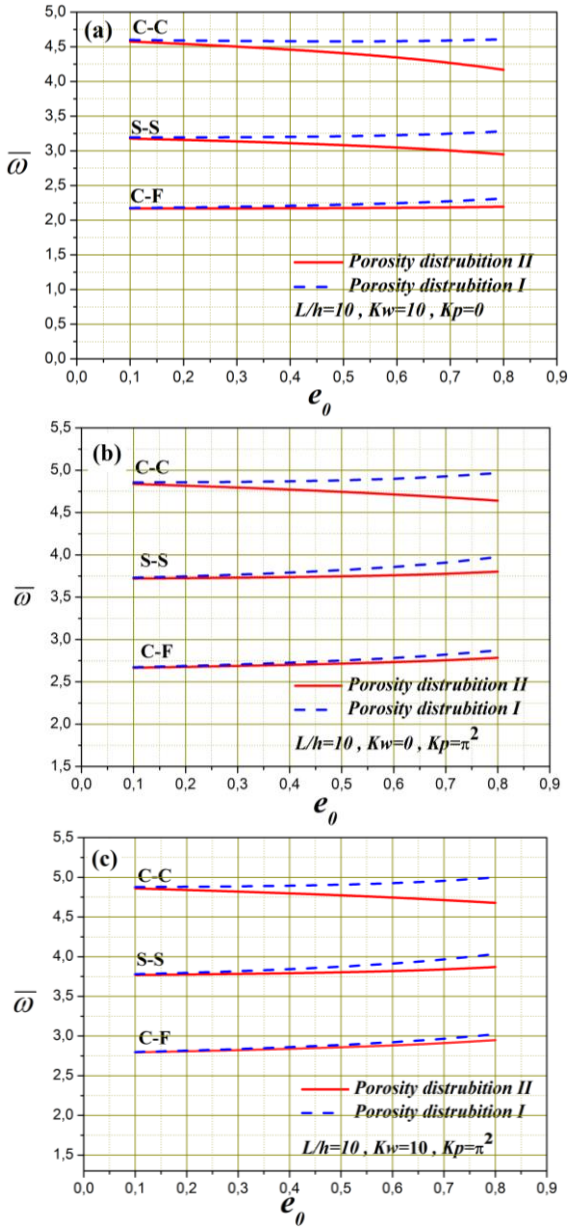

Fig. 7 Variation of the non-dimensional fundamental frequency of porous beams on the elastic foundation as a function of porosity parameters for various boundary conditions : (a) K_w=10 and K_p=0, (b) K_w=0 and K_p=π^2 and (c) K_w=10 and K_p=π^2

obtained non-dimensional frequencies of porous beams, as the slenderness ratio rise, indicating the porous beam is more pronounced and less resistance to vibrations. This effect is stabilized at higher slenderness ratios, suggesting the point when the vibration remains not influenced significantly due to slenderness. The porosity parameter introduces further complexity to the vibration analysis. Different types of porosity distributions react differently to increases in porosity. While Type-II porosity shows a gradual decline in fundamental frequency values, indicating a dampening effect on vibration, the impact overall remains marginal except at higher porosity levels. The introduction of elastic foundations such as Winkler and Pasternak

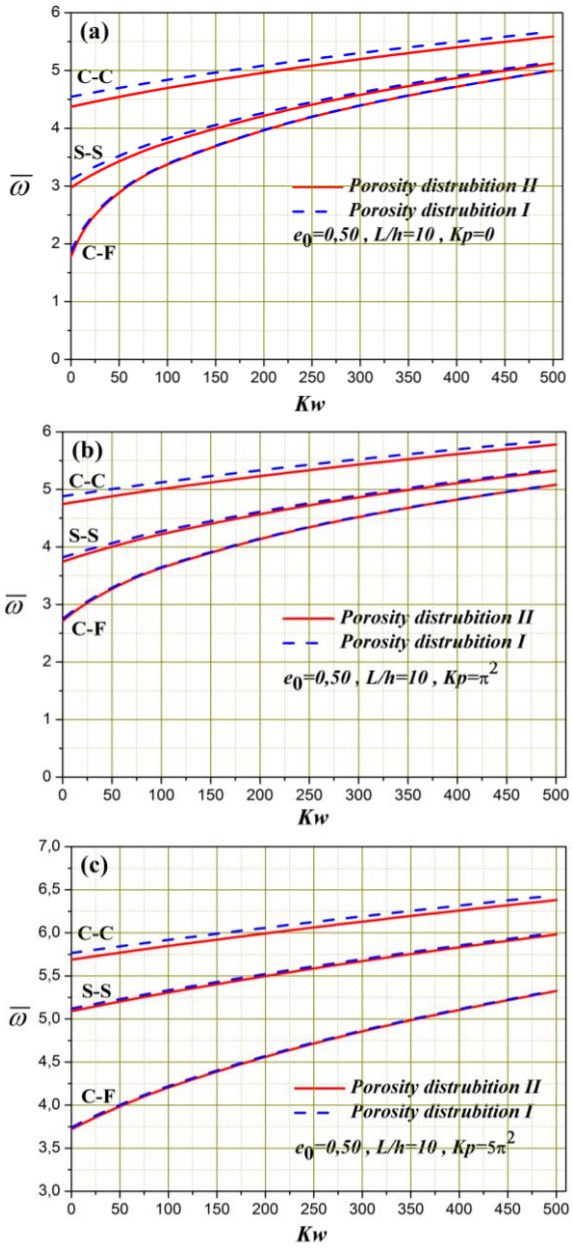

Fig. 8 Variation of the non-dimensional fundamental frequency of porous beams with various Winkler parameters and boundary conditions (L/h=10, $e0$=0.5): (a) K_p=0, (b) K_p=π^2 and (c) K_p=5π^2

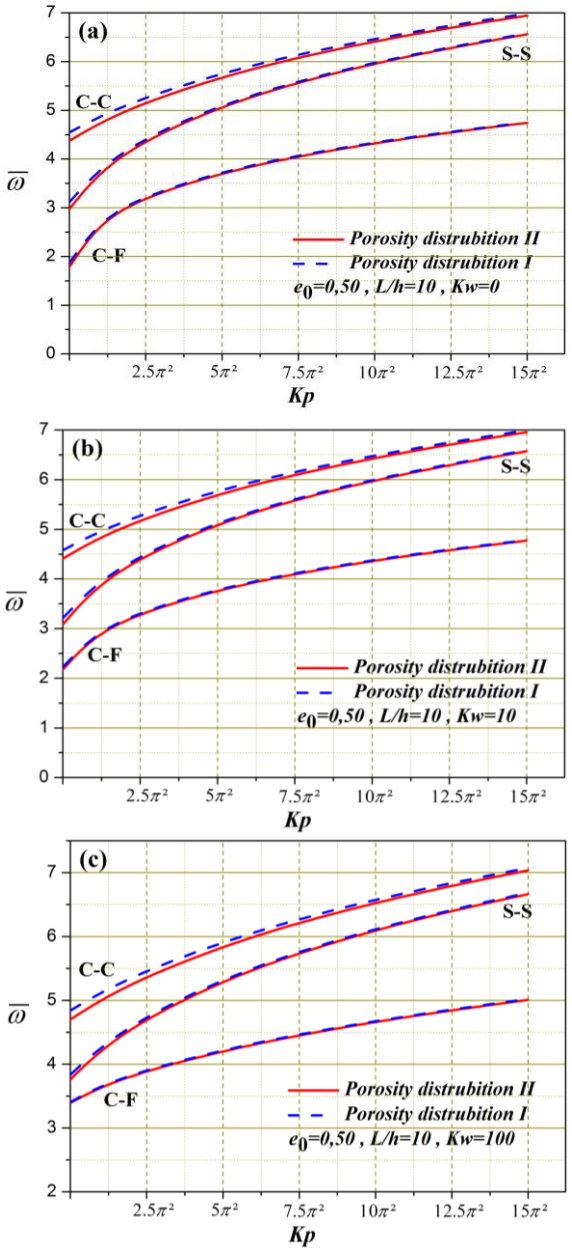

Fig. 9 Variation of the non-dimensional fundamental frequency of porous beams with various Pasternak parameters and boundary conditions (L/h=10, $e0$=0.5) : (a) K_w=0, (b) K_w=10 and (c) K_w=100

modifies the vibrational response of the beams. These foundations increase the stiffness and, consequently, the fundamental frequency of the beams, indicating a direct link between the foundation type and the vibrational characteristics of porous beams. The sensitivity of these effects varies with different boundary conditions, highlighting the importance of considering support constraints in vibration analysis.

5.3 Results for buckling analysis

Continuously, the non-dimensional critical buckling loads of isotropic beams with various Winkler and Pasternak coefficients and different boundary conditions are examined and compared to those obtained by Nguyen *et al*. (2023), Nguyen *et al*. (2022) and Naidu and Rao (1995). The numerical results are presented in Table 8. The obtained results are in excellent agreement with those given in the references, which are based on a refined shear deformation and Euler- Bernoulli beam theories, both theories are sufficient to simulate the mechanical behavior of a slenderness beam resting on elastic foundations. As previously stated, the compared results with Nguyen *et al*. (2022) and Nguyen *et al*. (2023) are based on refined shear deformation beam theories using the Ritz and Legendre-Ritz approximations, respectively, unlike the finite element method, which has a limit on the number of admissible function terms to avoid numerical instability. The number of

Table 8 Comparison of the non-dimensional buckling critical loads $\hat{P}_{cr}$ of isotropic beams with various boundary conditions and Winkler-Pasternak elastic foundation parameters (L/h=50)

BCs	K_W	K_P	Theories			
			Present	Nguyen *et al*. (2023)	Nguyen *et al*. (2022)	Naidu and Rao (1995)
S-S	0	0	9.8595	9.8595	9.9023	9.8696
		π^2	19.7291	19.7291	19.7195	19.739
		2.5 π^2	34.5335	34.5335	34.3413	34.544
	1	0	9.9608	9.9608	10.0035	9.9709
		π^2	19.8304	19.8304	19.8210	19.841
		2.5 π^2	34.6348	34.6348	34.4432	34.645
	102	0	19.9916	19.9916	20.0341	20.002
		π^2	29.8612	29.8612	29.8794	29.847
		2.5 π^2	44.6656	44.6656	44.5431	44.676
C-F	0	0	2.4668	2.4672	2.4694	2.4674
		π^2	12.3364	12.3368	12.3049	12.337
		2.5 π^2	27.1408	27.1412	26.9536	27.141
	1	0	2.6493	2.6498	2.6552	2.6499
		π^2	12.5189	12.5194	12.4880	12.520
		2.5 π^2	27.3233	27.3238	27.1373	27.324
	102	0	11.9827	12.0058	12.0438	11.996
		π^2	21.8523	21.8755	21.8810	21.866
		2.5 π^2	36.6567	36.6799	36.5324	36.670
C-C	0	0	39.3172	39.3170	/	39.479
		π^2	49.1868	49.1866	/	49.349
		2.5 π^2	63.9912	63.9910	/	64.153
	1	0	39.3931	39.3930	/	39.555
		π^2	49.2627	49.2626	/	49.425
		2.5 π^2	64.0671	64.0670	/	64.229
	102	0	46.8430	46.8429	/	47.007
		π^2	56.7126	56.7125	/	56.877
		2.5 π^2	71.5170	71.5169	/	71.681

generated unknowns makes the Ritz method unstable due to round-off errors. The developed element is efficient in analyzing the buckling of isotropic beams on elastic foundations. Isotropic beams on Pasternak elastic foundations are more susceptible to buckling than those on Winkler elastic foundations. The Pasternak model, which considers shear deformation, offers a more precise analysis. Beams on both foundations are sensitive to variations, but the Pasternak model offers higher buckling resistance due to its consideration of shear resistance. Overall, the Pasternak model offers higher resistance and sensitivity. The following example investigates the effect of porosity distribution patterns and slenderness ratios on the non-dimensional critical buckling loads for FGP beams without elastic foundations and subjected to different boundary conditions. Table 9 displays and compares the obtained results with those of Nguyen *et al*. (2023) and Nguyen *et al*. (2022) with a refined shear deformation beam theory, Chen *et al*. (2016), and Jamshidi and Arghavani (2018) with Timoshenko beam theory and using Ritz solutions. As has been shown previously, the proposed beam finite element achieves equivalent accuracy with both Lagrange and Hermite isoparametric formulations, highlighting the model's simplicity and ease of implementation in FGP beam buckling simulations.

Porosity patterns possess a significant impact on the computed non-dimensional buckling loads, with a significant discrepancy arising in the important length-to-thickness ratio (L/h=10) and lessening in slender beam cases, especially in the clamped-clamped boundary condition. The porosity pattern contributes to the reduction of the yielding stiffness and mass matrices, and the type-II porosity distribution pattern is of more concern. Table 10 displays the buckling loads of simply supported FGP beams for a range of Winkler and Pasternak foundation coefficients, including both Porosity I and Porosity II patterns. The results are consistent with those generated by a refined shear deformation beam theory with Legendre-Ritz solutions according to Nguyen *et al*. (2023). This correlation highlights the efficacy of the current beam element, which is based on both C0 and C1 interelement continuities, for predicting the buckling loads of FGP beams resting on Winkler and Pasternak elastic foundations.

This case study highlights the impact of Winkler and Pasternak elastic foundations on buckling critical loads, with a stiffer foundation provides high resistance to buckling. The obtained results demonstrate that porosity pattern type-I performs a greater magnitude of buckling critical loads compared to those given by porosity pattern type-II. For both porosity patterns, the buckling critical loads increase as the Winkler coefficient rises, referring to enhanced vertical rigidity of elastic foundations. Likewise, The Pasternak foundation also increases buckling critical

Table 9 Comparisons of the non-dimensional buckling load $\hat{P}_{cr}$ of porous functionally graded beams with various boundary conditions and slenderness ratios (*e0*=0.5)

BCs	*L/h*	Porosity Pattern	Theories				
			Present	Nguyen *et al*. (2023)	Nguyen *et al*. (2022)	Chen *et al*. (2016)	Jamshidi and Arghavani (2018)
S-S	10	Porosity I	0.012980	0.012953	0.012953	/	/
		Porosity II	0.010800	0.010800	/	/	/
	20	Porosity I	0.003337	0.003335	0.003335	0.003338	0.003339
		Porosity II	0.002760	0.002760	/	0.002869	/
C-F	10	Porosity I	0.003337	0.003335	0.003335	/	/
		Porosity II	0.002760	0.002760	/	/	/
	20	Porosity I	0.000840	0.000840	0.000840	0.000840	0.000840
		Porosity II	0.000694	0.000694		0.000694	/
C-C	10	Porosity I	0.046786	0.046433	0.046433	/	/
		Porosity II	0.039742	0.039735	/	/	/
	20	Porosity I	0.012980	0.012953	0.012953	0.013010	0.013010
		Porosity II	0.010800	0.010800	/	0.010806	/

Table 10 Comparisons of the non-dimensional buckling load $\overline{P}_{cr}$ of Simply-Supported porous functionally graded beams with various distribution patterns and Winkler-Pasternak elastic foundation parameters (*e0*=0.5 and *L/h*=15)

K_P	Porosity Pattern	Theories	K_W				
			0	10	50	100	500
0	Porosity I	Nguyen *et al*. (2023)	7.9609	8.9741	13.0269	18.0930	58.6215
		Present	7.9618	8.9750	13.0278	18.0939	58.6224
	Porosity II	Nguyen *et al*. (2023)	6.5978	7.6110	11.6639	16.7299	57.2584
		Present	6.5961	7.6093	11.6621	16.7282	57.2566*
π^2	Porosity I	Nguyen *et al*. (2023)	17.8305	18.8437	22.8965	27.9626	68.4911
		Present	17.8314	18.8446	22.8974	27.9635	68.4920
	Porosity II	Nguyen *et al*. (2023)	16.4674	17.4806	21.5335	26.5995	67.1280
		Present	16.4657	17.4789	21.5317	26.5978	67.1262*
2.5 π^2	Porosity I	Nguyen *et al*. (2023)	32.6349	33.6481	37.7009	42.7670	83.2955
		Present	32.6358	33.6490	37.7018	42.7679	83.2964
	Porosity II	Nguyen *et al*. (2023)	31.2718	32.2850	36.3379	41.4039	81.9324
		Present	31.2701	32.2833	36.3361	41.4022	81.9307*
5 π^2	Porosity I	Nguyen *et al*. (2023)	57.3089	58.3221	62.3749	67.4410	107.9695
		Present	57.3098	58.3230	62.3759	67.4419	107.9704
	Porosity II	Nguyen *et al*. (2023)	55.9458	56.9591	61.0119	66.0780	106.6064
		Present	55.9441	56.9573	61.0101	66.0762	106.6047*

* Obtained results are given for the second buckling mode

loads and highlighting the shear resistance for porous beams. This analysis highlights the key role induced by the combined effect of porosity distribution patterns and elastic foundations on the stability simulation. The buckling critical loads of porous beams with CC and CF boundary conditions are presented in Tables 11 and 12, respectively. Examination points to obtained results confirm an excellent agreement with those given by alternative approach of Nguyen *et al*. (2023). Table 11 shows that the non-dimensional buckling critical loads increase as both Winkler and Pasternak foundation coefficients increase. The results from the Present model are in close agreement with those from Nguyen *et al*. (2023), which indicates the accuracy and validity of the present beam element model. FGP Beams with the Porosity I pattern exhibit higher buckling loads compared to those with the Porosity II pattern, suggesting that the material characteristics with this porosity distribution are more resistant to buckling.

Table 12 also shows a similar trend where the non-dimensional buckling loads increase as the Winkler and Pasternak foundation coefficients increase for both Porosity I and Porosity II patterns. The Present model results are

Table 11 Comparisons of the non-dimensional buckling load $\overline{P}_{cr}$ of Simply-Supported porous functionally graded beams with various distribution patterns and Winkler-Pasternak elastic foundation parameters (*e0*=0.5 and *L/h*=15)

K_P	Porosity Pattern	Theories	K_W				
			0	10	50	100	500
0	Porosity I	Nguyen *et al*. (2023)	30.4501	31.2088	34.2174	37.9169	64.3403
		Present	30.4633	31.2219	34.2308	37.9307	64.3695
	Porosity II	Nguyen *et al*. (2023)	25.5178	26.2764	29.2816	32.9694	58.7746
		Present	25.4913	26.2499	29.2550	32.9422	58.7186
π^2	Porosity I	Nguyen *et al*. (2023)	40.3197	41.0784	44.0870	47.7865	74.2099
		Present	40.3329	41.0915	44.1004	47.8003	74.2391
	Porosity II	Nguyen *et al*. (2023)	35.3875	36.1460	39.1512	42.8390	68.6442
		Present	35.3610	36.1195	39.1246	42.8118	68.5882
2.5 π^2	Porosity I	Nguyen *et al*. (2023)	55.1241	55.8828	58.8914	62.5909	89.0143
		Present	55.1373	55.8959	58.9048	62.6047	89.0435
	Porosity II	Nguyen *et al*. (2023)	50.1919	50.9504	53.9557	57.6434	83.4486
		Present	50.1654	50.9239	53.9290	57.6162	83.3926
5 π^2	Porosity I	Nguyen *et al*. (2023)	79.7981	80.5568	83.5655	87.2649	113.6883
		Present	79.8113	80.5700	83.5788	87.2787	113.7175
	Porosity II	Nguyen *et al*. (2023)	74.8659	75.6244	78.6297	82.3174	108.1227
		Present	74.8394	75.5979	78.6030	82.2902	108.0666

Table 12 Comparisons of the non-dimensional buckling load $\overline{P}_{cr}$ of Clamped-Free porous functionally graded beams with various distribution patterns and Winkler-Pasternak elastic foundation parameters (*e0*=0.5 and *L/h*=15)

K_P	Porosity Pattern	Theories	K_W				
			0	10	50	100	500
0	Porosity I	Nguyen *et al*. (2023)	2.0134	3.6900	7.8607	10.4429	20.1009
		Present	2.0133	3.6896	7.8583	10.4375	20.0641
	Porosity II	Nguyen *et al*. (2023)	1.6638	3.3094	7.0805	9.3132	18.2681
		Present	1.6636	3.3087	7.0753	9.3034	18.2189
π^2	Porosity I	Nguyen *et al*. (2023)	11.8830	13.5596	17.7303	20.3125	29.9705
		Present	11.8829	13.5593	17.7279	20.3071	29.9337
	Porosity II	Nguyen *et al*. (2023)	11.5334	13.1790	16.9501	19.1828	28.1377
		Present	11.5332	13.1783	16.9449	19.1730	28.0885
2.5 π^2	Porosity I	Nguyen *et al*. (2023)	26.6874	28.3640	32.5347	35.1169	44.7749
		Present	26.6873	28.3637	32.5323	35.1115	44.7382
	Porosity II	Nguyen *et al*. (2023)	26.3378	27.9835	31.7545	33.9872	42.9421
		Present	26.3376	27.9827	31.7494	33.9774	42.8929
5 π^2	Porosity I	Nguyen *et al*. (2023)	51.3614	53.0380	57.2087	59.7909	69.4489
		Present	51.3613	53.0377	57.2063	59.7855	69.4122
	Porosity II	Nguyen *et al*. (2023)	51.0118	52.6575	56.4285	58.6612	67.6161
		Present	51.0116	52.6568	56.4234	58.6514	67.5669

again in close agreement with those from Nguyen *et al*. (2023). However, the difference in buckling loads between Porosity I and Porosity II patterns is less pronounced in the Clamped-Free case compared to the Clamped-Clamped case. The Winkler foundation coefficient can provide more stiffness and resist the lateral deflection that leads to buckling.

As a result, when the Winkler coefficient increases, the non-dimensional buckling load also increases, as seen in both Table 11 and Table 12. The FGP beam becomes more resistant to buckling as the foundation offers more support. The Pasternak foundation coefficient, which measures shear deformation between foundation layers, indicates the foundation's ability to transmit shear forces, contributing to

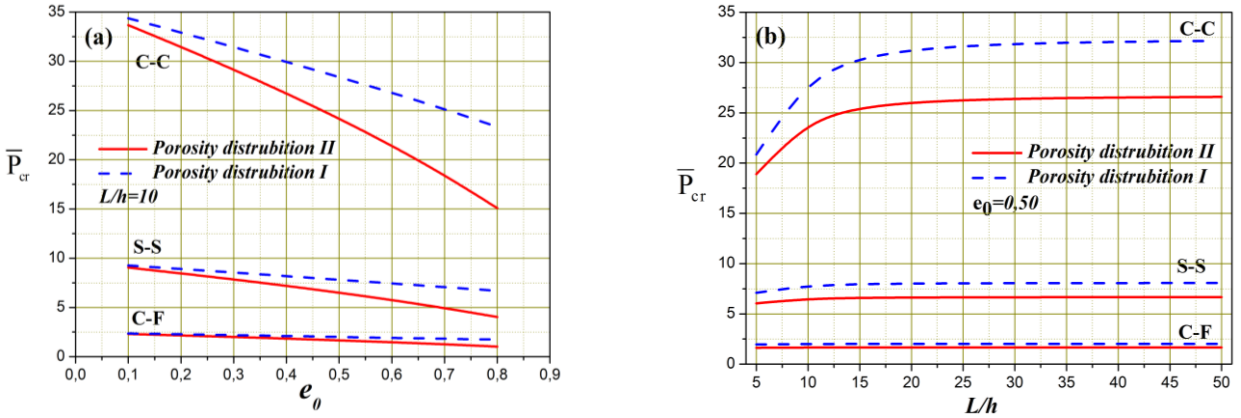

Fig. 10 Variation of the non-dimensional critical buckling load of porous beams without elastic foundations as a function of porosity parameters (a) and slenderness ratios (b) for various boundary conditions

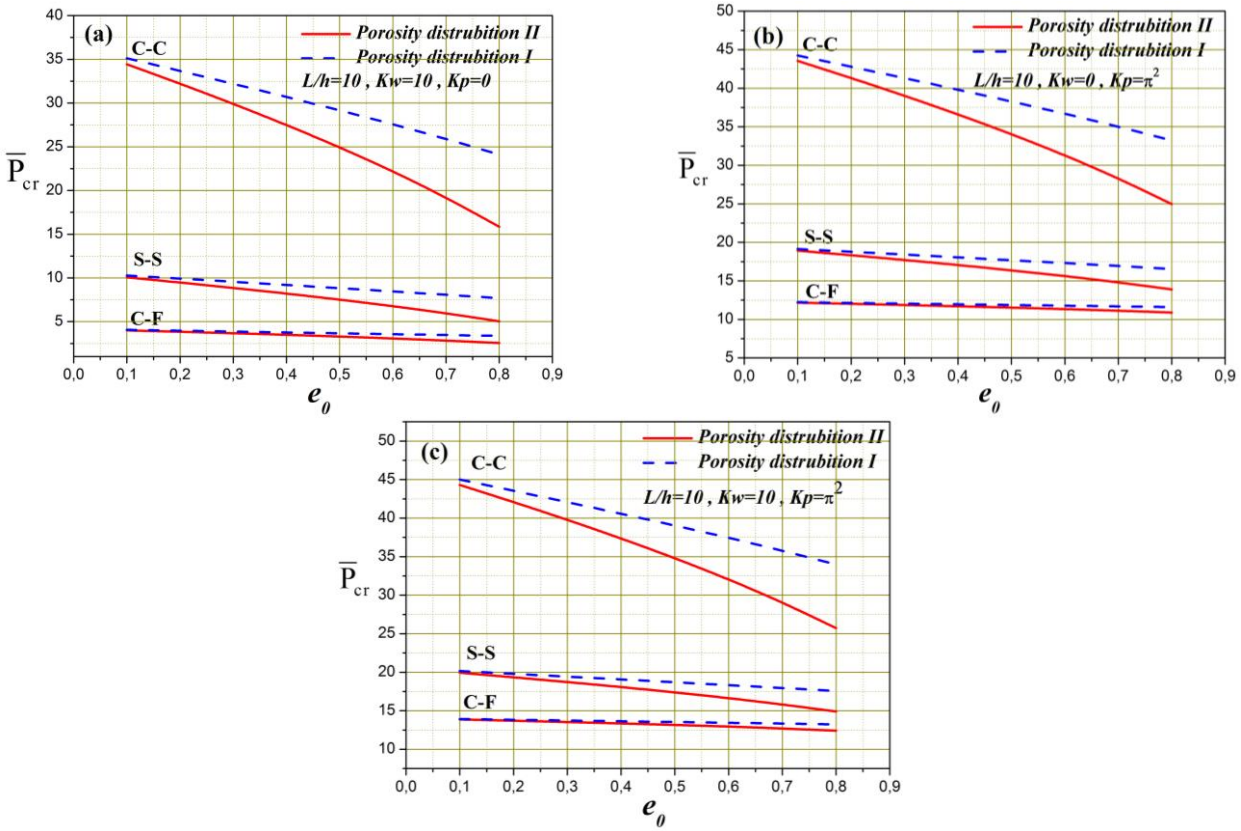

Fig. 11 Variation of the non-dimensional buckling critical load of porous beams on the elastic foundation as a function of porosity parameters for various boundary conditions: (a) K_w=10 and K_p=0, (b) K_w=0 and K_p=π^2 and (c) K_w=10 and K_p=π^2

its stiffness. An increase in the Pasternak coefficient increases the non-dimensional buckling load for both Clamped-Clamped and Clamped-Free cases. The Winkler elastic foundation has a larger impact on predicted buckling loads, especially for the Porosity I pattern, and is more significant for the stability of Clamped-Clamped and Clamped-Free boundary conditions of porous beams. The Pasternak elastic foundation is more critical for the stability of Clamped-Free beams, providing additional shear resistance. The specific effects of each foundation depend on the interplay between foundation properties and porous beam constraints.

In visual examination of the buckling behavior of porous beams, Figs. 10-13 illustrate the impact of slenderness ratios, porosity parameters, and the presence of elastic foundations on the critical buckling load. It is evident that as the slenderness ratio of the beam increases, so does its resistance to buckling. This relationship, however, plateaus beyond certain slenderness ratios, indicating a limit to the benefits of increased slenderness.

The porosity plays a crucial role in determining the buckling load, with significant decreases noted particularly in beams with Type-I porosity distribution as the porosity parameter increases. It is observed that the increasing in

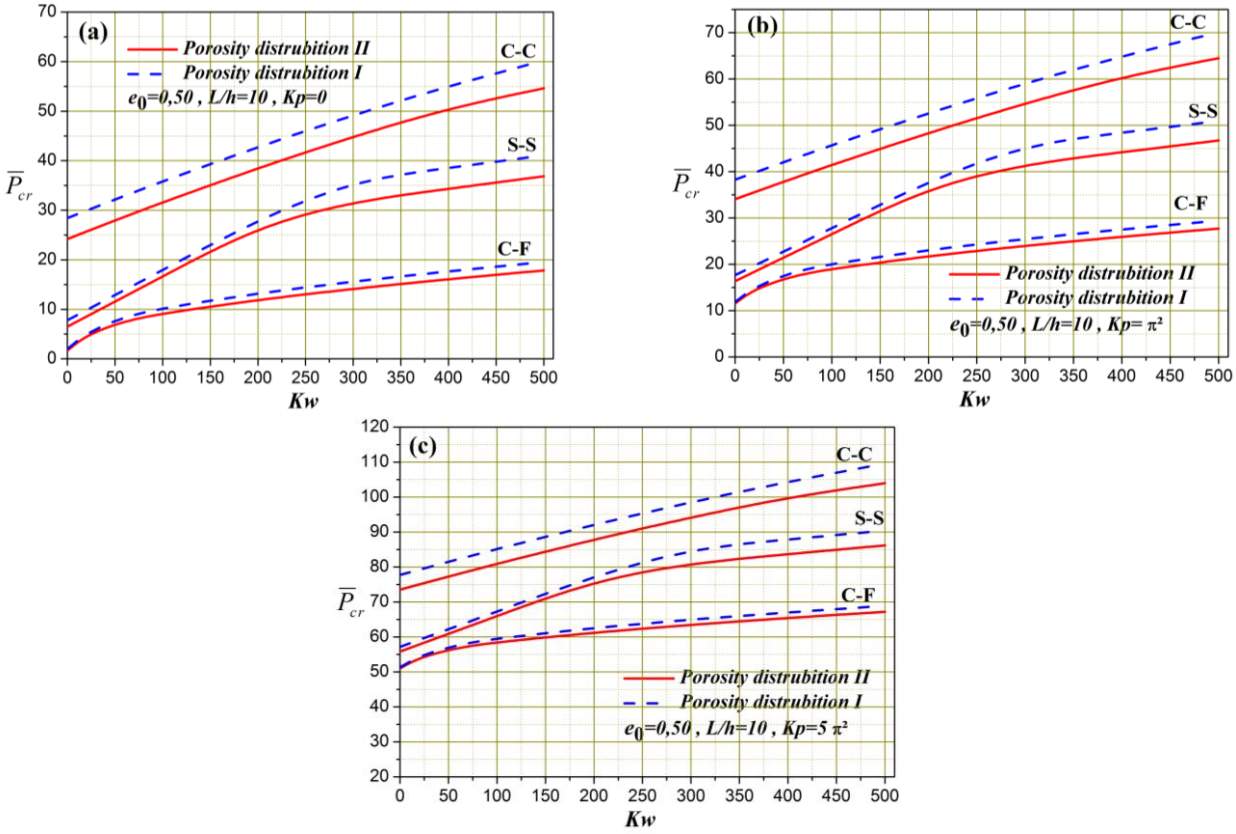

Fig. 12 Variation of the non-dimensional buckling critical load of porous beams with various Winkler parameters and boundary conditions (L/h=10, $e0$=0.5): (a) K_p=0, (b) K_p=π^2 and (c) K_p=5π^2.

porosity results in the stiffness's reduction, and therefore decrease the stability of the porous beam when subjected to compressive loads. Including both Winkler and Pasternak elastic foundations perform an enhancement of porous beams buckling resistance. When both elastic foundation coefficients rise, the porous beams prove more stability. The Pasternak foundation improves this stability more clearly, and porous beams resting on Pasternak foundation are less sensitive to buckling. These illustrations offer light on the combined effect of various parameters such as geometry, porosity gradation, and elastic foundations on the buckling analysis of porous functionally graded beams to optimum design and structural integrity.

6. Conclusions

The current study explores the combined effect of porosity and elastic foundation on the free vibration and buckling analysis of functionally graded porous beams. The formulated beam element is founded on a refined higher-order shear beam theory, combining Lagrange and Hermite interpolations to ensure interelement continuities and generate stiffness, geometry, and mass matrices from a weak form of Hamilton's variational principle. This research provides several insights, including the importance of porosity for optimal elastic properties and improved mechanical integrity. The Pasternak foundation parameter has a greater impact on critical buckling load and fundamental frequency than the Winkler foundation parameter, except for the Clamped-Clamped boundary condition. The symmetric distribution pattern is considered as favorable distribution pattern for investigating the free vibration response and providing more resistance to buckling critical loads. The current element is simple, efficient to implement numerically, and more stable in terms of stiffness, geometry, and mass matrices, offering an outline for the computational development of additional finite element models. The investigation also reveals that porosity's influence on frequencies depends on the appropriate distribution patterns, over the buckling analysis showing a trend of decreased critical loads. Both porosity and elastic foundation parameters play a sensitive role in predicted frequencies and bucking loads for porous beams. Finally, the current research sets for future explorations on functionally graded porous beams' mechanical responses resting on elastic foundations (Esen *et al*. 2021b, Abo-Bakr *et al*. 2020).

References

Abdelbari, S., Attia, A., Bourada, F., Bousahla, A.A., Tounsi, A. and Ghazwani, M.H. (2023), "Investigation of dynamic characteristics of imperfect FG beams on the Winkler–Pasternak foundation under thermal loading", *Phys. Mesomech*., **26**(5), 557-572. https://doi.org/10.1134/S1029959923050089.

Abo-Bakr, R.M., Eltaher, M.A. and Attia, M.A. (2020), "Pull-in

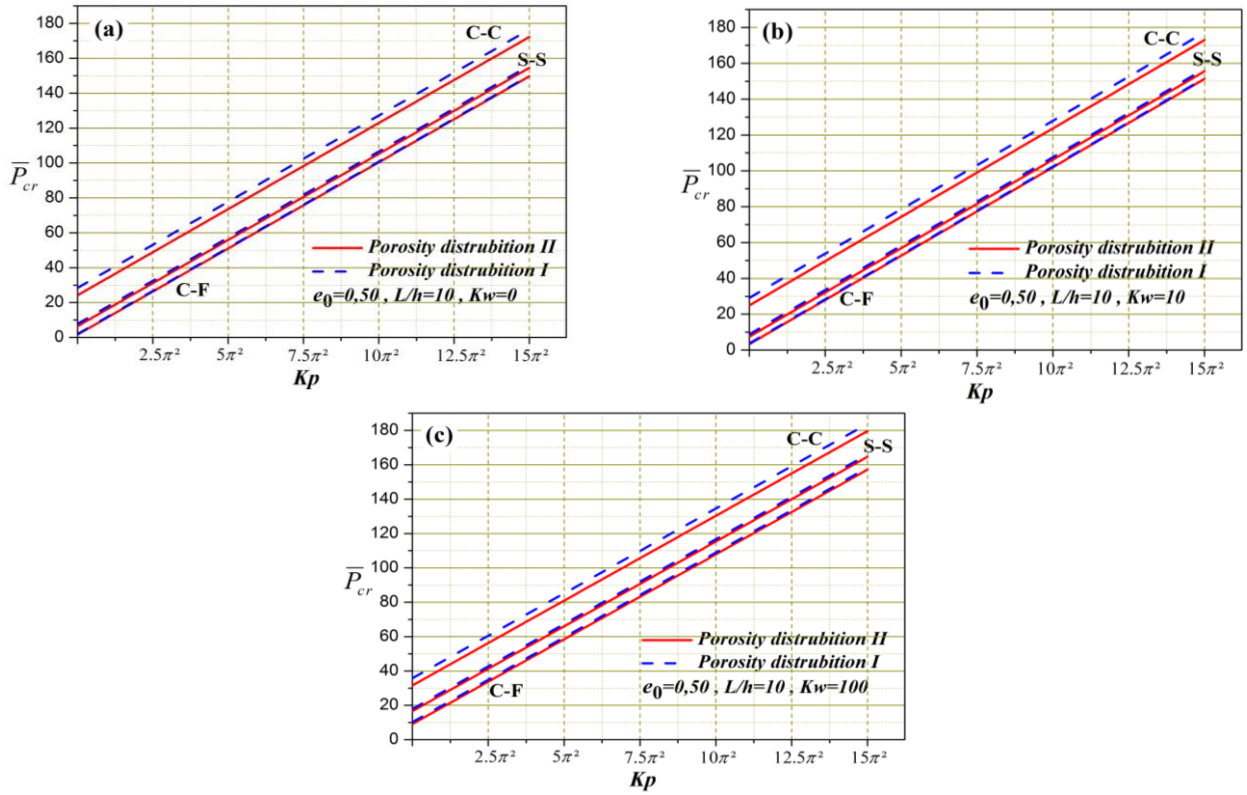

Fig. 13 Variation of the non-dimensional buckling critical load of porous beams with various Pasternak parameters and boundary conditions (L/h=10, $e0$=0.5) : (a) K_w=0, (b) K_w=10 and (c) K_w=100

and freestanding instability of actuated functionally graded nanobeams including surface and stiffening effects", *Eng. Comput*., 1-22. https://doi.org/10.1007/s00366-020-01146-0.

Adiyaman, G., Öner, E., Yaylaci, M. and Birinci, A. (2023), "A study on the contact problem of a layer consisting of functionally graded material (FGM) in the presence of body force", *J. Mech. Mat. Struct*., **18**(1), 125-141. https://doi.org/10.2140/jomms.2023.18.125.

Akbas, S.D., Fageehi, Y.A., Assie, A.E. and Eltaher, M.A. (2020a), "Dynamic analysis of viscoelastic functionally graded porous thick beams under pulse load", *Eng. Comput*., 1-13. https://doi.org/10.1007/s00366-020-01070-3.

Akbas, S.D., Bashiri, A.H., Assie, A.E. and Eltaher, M.A. (2020b), "Dynamic analysis of thick beams with functionally graded porous layers and viscoelastic support", *J. Vib. Control*, 1077546320947302. https://doi.org/10.1177/1077546320947302.

Ahmed, R.A., Fenjan, R.M. and Faleh, N.M. (2019), "Analyzing post-buckling behavior of continuously graded FG nanobeams with geometrical imperfections", *Geomech. Eng*., **17**(2), 175-180. https://doi.org/10.12989/gae.2019.17.2.175.

Ait Atmane, H., Tounsi, A. and Bernard, F. (2015), "Effect of thickness stretching and porosity on mechanical response of a functionally graded beams resting on elastic foundations", *Int .J. Mech. Mater. Design*, **13**(1), 71-84. https://doi.org/10.1007/s10999-015-9318-x.

Akbas, S.D. (2017), "Thermal effects on the vibration of functionally graded deep beams with porosity", *Int. J. Appl. Mech*., **9**(5), 1750076. https://doi.org/10.1142/S1758825117500764.

Al-Maliki, A.F., Faleh, N.M. and Alasadi, A.A. (2019), "Finite element formulation and vibration of nonlocal refined metal foam beams with symmetric and non-symmetric porosities", *Struct. Monit. Maint.,* **6**(2), 147-159. https://doi.org/10.12989/smm.2019.6.2.147.

Al-shujairi, M. and Mollamahmutoglu, C. (2018), "Buckling and free vibration analysis of functionally graded sandwich microbeams resting on elastic foundation by using nonlocal strain gradient theory in conjunction with higher order shear theories under thermal effect", *Compos. Part B: Eng*., **154**, 292-312. https://doi.org/10.1016/j.compositesb.2018.08.103.

Al-Toki, M.H., Ali, H.A., Faleh, N.M. and Fenjan, R.M. (2022), "Numerical assessment of nonlocal dynamic stability of graded porous beams in thermal environment rested on elastic foundation", *Geomech. Eng*., **28**(5), 455-461. https://doi.org/10.12989/gae.2022.28.5.455.

Alnujaie, A., Akbas, Ş.D., Eltaher, M.A. and Assie, A. (2021), "Forced vibration of a functionally graded porous beam resting on viscoelastic foundation", *Geomech. Eng*., **24**(1), 91-103. https://doi.org/10.12989/gae.2021.24.1.091.

Ansari, R., Faraji Oskouie, M., Nesarhosseini, S. and Rouhi, H. (2022), "Nonlinear thermally induced vibration analysis of porous FGM Timoshenko beams embedded in an elastic medium". *Transp. Porous Med*., **142**, 63-87. https://doi.org/10.1007/s00707-022-03455-5.

Arefi, M. and Zur, K.K. (2020), "Free vibration analysis of functionally graded cylindrical nanoshells resting on Pasternak foundation based on two-dimensional analysis", *Steel Compos. Struct*., **34**(4), 615-623. https://doi.org/10.12989/scs.2020.34.4.615.

Avcar, M. and Mohammed, W.K.M. (2018), "Free vibration of functionally graded beams resting on Winkler-Pasternak foundation", *Arab. J. Geosci*., **11**(10), 232. https://doi.org/10.1007/s12517-018-3579-2

Avcar, M. (2019), "Free vibration of imperfect sigmoid and power law functionally graded beams", *Steel Compos. Struct*., **30**(6), 603-615. https://doi.org/10.12989/scs.2019.30.6.603.

Assie, A.E., Mohamed, S.A., Shanab, R.A., Abo-bakr, R.M. and Eltaher, M.A. (2023), "Static buckling of 2D FG porous plates

resting on elastic foundation based on unified shear theories", *J. Appl. Comput. Mech*., **9**(1), 239-258. https://doi.org/10.22055/jacm.2022.41265.3723.

Babaei, H., Kiani, Y. and Żur, K.K. (2022), "New insights into nonlinear stability of imperfect nanocomposite beams resting on a nonlinear medium", *Commun. Nonlinear. Sci. Numer. Simul*., **118**,106993. https://doi.org/10.1016/j.cnsns.2022.106993.

Bashiri, A.H., Akbas, S.D., Abdelrahman, A.A., Assie, A., Eltaher, M.A. and Mohamed, E.F. (2021), "Vibration of multilayered functionally graded deep beams under thermal load", *Geomech. Eng.*, **24**(6), 545-557. https://doi.org/10.12989/gae.2021.24.6.545.

Belabed, Z., Selim, M.M., Slimani, O., Taibi, N., Tounsi, A. and Hussain, M. (2021), "An efficient higher order shear deformation theory for free vibration analysis of functionally graded shells", *Steel Compos. Struct.*, **40**(2), 307-321. https://doi.org/10.12989/scs.2021.40.2.307.

Chen, W.Q., Lu, C.F. and Bian, Z.G. (2004), "A mixed method for bending and free vibration of beams resting on a Pasternak elastic foundation", *Appl. Math. Model*., **28**(10), 877-890. https://doi.org/10.1016/j.apm.2004.04.001.

Chen, D., Yang, J. and Kitipornchai, S. (2015), "Elastic buckling and static bending of shear deformable functionally graded porous beam", *Compos. Struct*., **133**, 54-61. https://doi.org/10.1016/j.compstruct.2015.07.052.

Chen, D., Yang, J. and Kitipornchai, S. (2016), "Free and forced vibrations of shear deformable functionally graded porous beams", *Int. J. Mech. Sci*., **108**, 14-22. https://doi.org/10.1016/j.ijmecsci.2016.01.025.

Dhatt, G., Lefrancois, E. and Touzot, G. (2012). Finite Element Method, *ISTE Ltd and John Wiley & Sons Inc*. https://doi.org/10.1002/9781118569764.

Duc, N.D. and Thang, P.T. (2015), "Nonlinear dynamic response and vibration of shear deformable imperfect eccentrically stiffened S-FGM circular cylindrical shells surrounded on elastic foundations", *Aerosp. Sci. Technol*., **40**, 115-127. https://doi.org/10.1016/j.ast.2014.11.005.

Ebrahimi, F. and Jafari, A. (2016), "Thermo-mechanical vibration analysis of temperature-dependent porous FG beams based on Timoshenko beam theory", *Struct. Eng. Mech*., **59**(2), 343-371. https://doi.org/10.12989/sem.2016.59.2.343.

Ebrahimi, F. and Dabbagh, A. (2019) "Vibration analysis of graphene oxide powder-/carbon fiber-reinforced multi-scale porous nanocomposite beams: a finite-element study", *Eur. Phys. J. Plus*, **134**, 225. https://doi.org/10.1140/epjp/i2019-12594-1

Ebrahimi, F. and Seyfi, A. (2021) "A wave propagation study for porous metal foam beams resting on an elastic foundation", *Waves Random Complex.*, https://doi.org/10.1080/17455030.2021.1905909.

Esen, I., Abdelrhmaan, A.A. and Eltaher, M.A. (2021a), "Free vibration and buckling stability of FG nanobeams exposed to magnetic and thermal fields", *Eng. Comput*., 1-20. https://doi.org/10.1007/s00366-021-01389-5.

Esen, I., O Zarpa, C. and Eltaher, M.A. (2021b), "Free vibration of a cracked FG microbeam embedded in an elastic matrix and exposed to magnetic field in a thermal environment", *Compos. Struct*., **261**, 113552. https://doi.org/10.1016/j.compstruct.2021.113552.

Esen, I., Eltaher, M.A. and Abdelrahman, A.A. (2021c), "Vibration response of symmetric and sigmoid functionally graded beam rested on elastic foundation under moving point mass", *Mech. Based Des. Struc*., 1-25. https://doi.org/10.1080/15397734.2021.1904255.

Fallah, A. and Aghdam, M.M., (2023), "Physics-informed neural network for bending and free vibration analysis of three-dimensional functionally graded porous beam resting on elastic foundation", *Eng. Comput*., 1-18. https://doi.org/10.1007/s00366-023-01799-7.

Fan, F., Safaei, B. and Sahmani, S. (2021), "Buckling and postbuckling response of nonlocal strain gradient porous functionally graded micro/nano-plates via NURBS-based isogeometric analysis", *Thin Wall. Struct*., **159**, 107231. https://doi.org/10.1016/j.tws.2020.107231.

Fazzolari, F.A. (2018), "Generalized exponential, polynomial and trigonometric theories for vibration and stability analysis of porous FG sandwich beams resting on elastic foundations", *Compos. Part B: Eng*., **136**, 254-271. https://doi.org/10.1016/j.compositesb.2017.10.022.

Fouaidi, M., Belfallah, K., Jamal, M., and Belouaggadia, N. (2023), "Transient analysis of functionally graded graphene oxide powders-reinforced porous composite beams resting on elastic foundations using the reproducing kernel particle meshless method", *Eng. Anal. Bound. Elem*., **146**, 460-472. https://doi.org/10.1016/j.enganabound.2022.10.029.

Gao, K., Li, R. and Yang, J. (2019), "Dynamic characteristics of functionally graded porous beams with interval material properties", *Eng. Struct*., **197**, 109441. https://doi.org/10.1016/j.engstruct.2019.109441.

Ghandourah, E. E., Ahmed, H. M., Eltaher, M. A., Attia, M. A. and Abdraboh, A. M. (2021), "Free vibration of porous FG nonlocal modified couple nanobeams via a modified porosity model", *Adv. Nano Res*., **11**(4), 405-422. https://doi.org/10.12989/anr.2021.11.4.405.

Ghorbanpour Arani, A., Khani, M. and Khoddami Maraghi, Z. (2018), "Dynamic analysis of a rectangular porous plate resting on an elastic foundation using high-order shear deformation theory", *J. Vib. Control*, **24**, 3698-3713. https://doi.org/10.1177/1077546317709388.

Huang, W. and Tahouneh, V. (2021), "Frequency study of porous FGPM beam on two-parameter elastic foundations via Timoshenko theory", *Steel Compos. Struct*., **40**(1), 139-156. https://doi.org/10.12989/scs.2021.40.1.139.

Jamshidi, M., Arghavani, J. and Maboudi, G. (2019), "Post-buckling optimization of two-dimensional functionally graded porous beams", *Int. J. Mech. Mater*., **15**, 801-815. https://doi.org/10.1007/s10999-019-09443-3.

Jamshidi, M. and Arghavani, J. (2018), "Optimal material tailoring of functionally graded porous beams for buckling and free vibration behaviors", *Mech. Res. Commun*., **88**, 19-24. https://doi.org/10.1016/j.mechrescom.2018.01.006.

Jalaei, M.H. and Civalek, O. (2019), "On dynamic instability of magnetically embedded viscoelastic porous FG nanobeams", *Int. J. Eng. Sci.,* **143**, 14-32. https://doi.org/10.1016/j.ijengsci.2019.06.013.

Jena, S.K., Chakraverty, S. and Malikan, M. (2020), "Application of shifted Chebyshev polynomial-based Rayleigh-Ritz method and Navier's technique for vibration analysis of a functionally graded porous beam embedded in Kerr foundation", *Eng. Comput*., 1-21. https://doi.org/10.1007/s00366-020-01018-7.

Jena, S. K., Chakraverty, S., Mahesh, V. and Harursampath, D., (2022), "Wavelet-based techniques for Hygro-Magneto-Thermo vibration of nonlocal strain gradient nanobeam resting on Winkler-Pasternak elastic foundation", *Eng. Anal. Bound. Elem*., **140**, 494–506. https://doi.org/10.1016/j.enganabound.2022.04.037

Hamed, M.A., Mohamed, S.A. and Eltaher, M.A. (2020), "Buckling analysis of sandwich beam rested on elastic foundation and subjected to varying axial in-plane loads", *Steel Compos. Struct*., **34**(1), 75-89. https://doi.org/10.12989/scs.2020.34.1.075.

Khoram, M.M., Hosseini, M., Hadi, A. and Shishehsaz, M. (2020), "Bending analysis of bidirectional FGM Timoshenko nanobeam subjected to mechanical and magnetic forces and resting on

Winkler-Pasternak foundation", *Int. J. Appl. Mech*., **12**(8), 2050093. https://doi.org/10.1142/S1758825120500933.

Lee, W.H., Han, S.C. and Park, W.T. (2015), "A refined higher order shear and normal deformation theory for E-, P-, and SFGM plates on Pasternak elastic foundation", *Compos. Struct*., **122**, 330-342. https://doi.org/10.1016/j.compstruct.2014.11.047.

Liu, H., Liu, H. and Yang, J. (2018), "Vibration of FG magnetoelectro-viscoelastic porous nanobeams on visco-Pasternak foundation", *Compos. Part B Eng*., **155**, 244-256. https://doi.org/10.1016/j.compositesb.2018.08.042

Madenci, E. (2021), "Free vibration and static analyses of metal-ceramic FG beams via high-order variational MFEM", *Steel Compos. Struct*., **39**(5), 493-509. https://doi.org/10.12989/scs.2021.39.5.493.

Mehala, T., Belabed, Z., Tounsi, A. and Beg, O.A. (2018), "Investigation of influence of homogenization models on stability and dynamic of FGM plates on elastic foundations", *Geomech. Eng*., **16**(3), 257-271. https://doi.org/10.12989/gae.2018.16.3.257.

Melaibari, A., Abo-bakr, R.M., Mohamed, S.A. and Eltaher, M.A. (2020), "Static stability of higher order functionally graded beam under variable axial load", *Alex. Eng. J*., **59**(3), 1661-1675. https://doi.org/10.1016/j.aej.2020.04.012.

Melaibari, A., Mohamed, S. A., Assie, A.E., Shanab, R.A. and Eltaher, M.A. (2022), "Free vibration characteristics of bidirectional graded porous plates with elastic foundations using 2D-DQM", *Mathematics*, **11**(1), 46. https://doi.org/10.3390/math11010046.

Mohamed, S.A., Mohamed, N. and Eltaher, M.A. (2022), "Snap-through instability of helicoidal composite imperfect beams surrounded by nonlinear elastic foundation", *Ocean Eng*., **263**, 112171. https://doi.org/10.1016/j.oceaneng.2022.112171.

Naidu, N.R. and Rao, G.V. (1995), "Stability behaviour of uniform columns on a class of two parameter elastic foundation", *Comput. Struct*., **57**(3), 551-553. https://doi.org/10.1016/0045-7949(94)00636-H.

Nguyen, N.D., Nguyen, T.N., Nguyen, T.K. and Vo, T.P. (2022), "A new two-variable shear deformation theory for bending, free vibration and buckling analysis of functionally graded porous beams", *Compos. Struct*., **282**, 115095. https://doi.org/10.1016/j.compstruct.2021.115095.

Nguyen, N.D., Nguyen, T.N., Nguyen, T.K. and Vo, T.P. (2023), "A Legendre-Ritz solution for bending, buckling and free vibration behaviours of porous beams resting on the elastic foundation". *Struct*., **50**, 1934-1950. https://doi.org/10.1016/j.istruc.2023.03.018.

Oner, E., Sengul Sabano, B., Uzun Yaylaci, E., Adiyaman, G., Yaylaci, M. and Birinci, A. (2022), "On the plane receding contact between two functionally graded layers using computational, finite element and artificial neural network methods", ZAMM - *J. Appl. Math. Mech*., **102**(2), e202100287. https://doi.org/10.1002/zamm.202100287.

Ozdemir, M.E. and Yaylaci, M, (2023), "Research of the impact of material and flow properties on fluid-structure interaction in cage systems", *Wind Struct*., **36**(1), 31-40. https://doi.org/10.12989/was.2023.36.1.031.

Pham, Q.H., Tran, V.K. and Nguyen, P.C. (2022), "Hygro-thermal vibration of bidirectional functionally graded porous curved beams on variable elastic foundation using generalized finite element method", *Case Stud. Therm. Eng.*, **40**, 102478. https://doi.org/10.1016/j.csite.2022.102478.

Rachedi, M.A., Benyoucef, S., Bouhadra, A., Bachir Bouiadjra, R., Sekkal, M. and Benachour, A. (2020), "Impact of the homogenization models on the thermoelastic response of FG plates on variable elastic foundation",*Geomech. Eng.*, **22**(1), 65-80. https://doi.org/10.12989/gae.2020.22.1.065.

Setoodeh, A. and Rezaei, M. (2017), "Large amplitude free vibration analysis of functionally graded nano/micro beams on nonlinear elastic foundation", *Struct. Eng. Mech*., **61**(2), 209-220. https://doi.org/10.12989/sem.2017.61.2.209.

Shanab, R., Mohamed, S., Tharwan, M.Y., Assie, A.E. and Eltaher, M.A. (2022), "Buckling of 2D FG Porous unified shear plates resting on elastic foundation based on neutral axis", *Steel Compos. Struct*., **45**(5), 729-747. https://doi.org/10.12989/scs.2022.45.5.729

Turan, M., Uzun Yaylaci, E. and Yaylaci, M. (2023), "Free vibration and buckling of functionally graded porous beams using analytical, finite element, and artificial neural network methods", *Arch. Appl. Mech*., **93**, 1351-1372. https://doi.org/10.1007/s00419-022-02332-w.

Uzun, B., Civalek, Ö. and Yayli, M.Ö., (2020), "Vibration of FG nano-sized beams embedded in Winkler elastic foundation and with various boundary conditions", *Mech. Based Des. Struc*., *Mach.*, 1-20. https://doi.org/10.1080/15397734.2020.1846560.

Van Long, N., Nguyen, V.L., Tran, M.T. and Thai, D.K. (2022), "Exact solution for nonlinear static behaviors of functionally graded beams with porosities resting on elastic foundation using neutral surface concept", *Proc. Inst. Mech. Eng. Part C*, **236**(1), 481-495. https://doi.org/10.1177/095440622110211.

Wang, Y., Xie, K., Fu, T. and Zhang, W. (2021), "A third order shear deformable model and its applications for nonlinear dynamic response of graphene oxides reinforced curved beams resting on visco-elastic foundation and subjected to moving loads", *Eng. Comput*., 1-15. https://doi.org/10.1007/s00366-020-01238-x.

Wu, D., Liu, A., Huang, Y., Huang, Y., Pi, Y. and Gao, W. (2018), "Dynamic analysis of functionally graded porous structures through finite element analysis", *Eng. Struct*., **165**, 287-301. https://doi.org/10.1016/j.engstruct.2018.03.023.

Xiao, H., Yan, K.M. and She, G. (2021), "Study on the characteristics of wave propagation in functionally graded porous square plates", *Geomech. Eng*., **26**(6), 607-615. https://doi.org/10.12989/gae.2021.26.6.607.

Xin, L. and Kiani, Y. (2023), "Vibration characteristics of arbitrary thick sandwich beam with metal foam core resting on elastic medium", *Struct*., **49**, 1-11. https://doi.org/10.1016/j.istruc.2023.01.108.

Yaylaci, M. (2016), "The investigation crack problem through numerical analysis", *Struct. Eng. Mech*., **57**(6), 1143-1156. https://doi.org10.12989/sem.2016.57.6.1143.

Yaylaci, M., Yayli, M., Yaylaci, E.U., Olmez, H. and Birinci, A. (2021), "Analyzing the contact problem of a functionally graded layer resting on an elastic half plane with theory of elasticity, finite element method and multilayer perceptron", *Struct. Eng. Mech*., **78**(5), 585-597. https://doi.org/10.12989/sem.2021.78.5.585.

Yaylaci, M., Sabano, B.S., Ozdemir, M.E. and Birinci, A. (2022a), "Solving the contact problem of functionally graded layers resting on a HP and pressed with a uniformly distributed load by analytical and numerical methods", *Struct. Eng. Mech*., **82**(3), 401-416. https://doi.org/10.12989/sem.2022.82.3.401.

Yaylaci, M., Abanoz, M., Yaylaci, E.U., Olmez, H., Sekban, D.M. and Birinci, A. (2022b), "Evaluation of the contact problem of functionally graded layer resting on rigid foundation pressed via rigid punch by analytical and numerical (FEM and MLP) methods", *Arch. Appl. Mech*., **92**(6), 1953-1971. https://doi.org/10.1007/s00419-022-02159-5.

Yaylaci, M. (2022c), "Simulate of edge and an internal crack problem and estimation of stress intensity factor through finite element method", *Adv. Nano Res*., **12**(4), 405-414. https://doi.org/10.12989/anr.2022.12.4.405.

Yaylaci, M., Yaylaci, E.U., Ozdemir, M.E., Ay, S. and Ozturk, S. (2022d), "Implementation of finite element and artificial neural network methods to analyze the contact problem of

a functionally graded layer containing crack", *Steel Compos. Struct*., **45**(4), 501-511. https://doi.org/10.12989/scs.2022.45.4.501.

Yaylaci, E.U., Oner, E., Yaylaci, M., Ozdemir, M.E., Abushattal, A. and Birinci, A. (2022e), "Application of artificial neural networks in the analysis of the continuous contact problem", *Struct. Eng. Mech*., **84**(1), 35-48. https://doi.org/10.12989/sem.2022.84.1.035.

Yaylaci, M., Abanoz, M., Yaylaci, E.U., Olmez, H., Sekban, D.M. and Birinci, A. (2022f), "The contact problem of the functionally graded layer resting on rigid foundation pressed via rigid punch", *Steel Compos. Struct*., **43**(5), 661-672. https://doi.org/10.12989/scs.2022.43.5.661.

Yaylaci, M., Yaylaci, E.U., Ozdemir, M.E., Ozturk, S. and Sesli, H. (2023), "Vibration and buckling analyses of FGM beam with edge crack: Finite element and multilayer perceptron methods", *Steel Compos. Struct*., **46**(4), 565-575. https://doi.org/10.12989/scs.2023.46.4.565.

Ying, J., Lu, C.F. and Chen, W.Q. (2008), "Two-dimensional elasticity solutions for functionally graded beams resting on elastic foundations", *Compos. Struct*., **84**(3), 209-219. https://doi.org/10.1016/j.compstruct.2007.07.004.

Zienkiewicz, O.Z., Taylor, R.L. and Zhu, J.Z. (2005), The Finite Element Method: Its Basis and Fundamentals, 6th Ed., Singapore.

Zhang, B., He, Y., Liu, D., Shen, L. and Lei, J. (2015), "An efficient size-dependent plate theory for bending, buckling and free vibration analyses of functionally graded microplates resting on elastic foundation", *Appl. Math. Model*., **39**(13), 3814-3845. https://doi.org/10.1016/j.apm.2014.12.001.

Zhang, L.H., Lai, S.K., Wang, C. and Yang, J. (2021), "DSC regularized Dirac-delta method for dynamic analysis of FG graphene platelet-reinforced porous beams on elastic foundation under a moving load", *Compos. Struct*., **255**, 112865. https://doi.org/10.1016/j.compstruct.2020.112865.

CC

Appendix A

The element stiffness matrix,

$$
\begin{aligned}
&[K]_m = \int_{-1}^{1}\left(B_m^T A_{11} B_m\right) J d\xi \;;\; [K]_{mb} = \int_{-1}^{1}\left(B_m^T B_{11} B_b\right) J d\xi \\
&[K]_{ms} = \int_{-1}^{1}\left(B_m^T B_{11}^s B_s\right) J d\xi \;;\; [K]_{bm} = \int_{-1}^{1}\left(B_s^T B_{11} B_m\right) J d\xi \\
&[K]_b = \int_{-1}^{1}\left(B_b^T D_{11} B_b\right) J d\xi \;;\; [K]_{bs} = \int_{-1}^{1}\left(B_b^T H_{11}^s B_s\right) J d\xi \\
&[K]_{sm} = \int_{-1}^{1}\left(B_s^T B_{11} B_m\right) J d\xi \;;\; [K]_{sb} = \int_{-1}^{1}\left(B_s^T D_{11} B_b\right) J d\xi \\
&[K]_s = \int_{-1}^{1}\left(B_s^T H_{11}^s B_s\right) J d\xi \;;\; \left[\overline{K}\right]_s = \int_{-1}^{1}\left(\overline{B}_s^T A_{44}^s \overline{B}_s\right) J d\xi \\
&[K]_W = k_W \int_{-1}^{1}\left(B_W^T B_W\right) J d\xi \;;\; [K]_p = k_p \int_{-1}^{1}\left(B_0^T B_0\right) J d\xi
\end{aligned}
\tag{35}
$$

The element geometric matrix

$$
[G] = \int_{-1}^{1}\left(B_0^T B_0\right) J d\xi \tag{36}
$$

The element mass matrix

$$
\begin{aligned}
&[M]_m = \int_{-1}^{1}\left(N^T I_1 N\right) J d\xi \quad ;[M]_b = \int_{-1}^{1}\left(H^T I_1 H\right) J d\xi \\
&[M]_{bm}^1 = -\int_{-1}^{1}\left(N^T I_2 H_{,x}\right) J d\xi \;;[M]_{mb}^1 = -\int_{-1}^{1}\left(H^T I_2 N_{,x}\right) J d\xi \\
&[M]_b^2 = \int_{-1}^{1}\left(H^T I_3 H_{,xx}\right) J d\xi \quad ;[M]_{bs} = \int_{-1}^{1}\left(N^T I_4 N\right) J d\xi \\
&[M]_{bs} = \int_{-1}^{1}\left(H^T I_5 N_{,x}\right) J d\xi \quad ;[M]_{sm} = -\int_{-1}^{1}\left(H^T I_5 N_{,x}\right) J d\xi \\
&[M]_{bs}^1 = -\int_{-1}^{1}\left(N^T I_5 H_{,x}\right) J d\xi \;;[M]_s = \int_{-1}^{1}\left(N^T I_6 N\right) J d\xi
\end{aligned}
\tag{37}
$$